Expert Systems With Applications 249 (2024) 123451

Contents lists available at ScienceDirect

Expert Systems With Applications

journal homepage: www.elsevier.com/locate/eswa

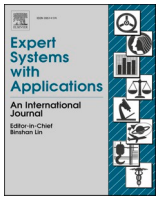

Freight rate index forecasting with Prophet model based on multi-dimensional significant events

Wenyang Wang [a,b,c,*], Nan He [a], Muxin Chen [a], Peng Jia [a,b]

[a] Collaborative Innovation Center for Transport Studies, Dalian Maritime University, Dalian 116026, China
[b] School of Maritime Economics and Management, Dalian Maritime University, Dalian 116026, China
[c] Dalian Institute of Chemical Physics, Chinese Academy of Sciences, Dalian 116026, China

ARTICLE INFO

Keywords:
BDI
Forecasting research
Prophet model
Significant event uncertainty indexes

ABSTRACT

The Baltic Dry Index (BDI) is an essential index to measure international dry bulk shipping freight, which can reflect global economic changes to a certain extent. Accurate forecasting of BDI supports shipping market participants in grasping risks and making scientific decisions. Based on the Prophet model, this paper considers the impact of multi-dimensional significant events related to the shipping industry and conducts BDI forecasting research. Firstly, we simulate the most momentous events in the world in recent years, namely the 2008 Global Financial Crisis and the 2019 New Crown Epidemic, and utilize the Prophet model to decompose the BDI sequence into three parts: trend, seasonality, and momentous event shocks. Secondly, we extensively collect other multi-dimensional significant event uncertainty indexes to establish a "significant event database". The Maximal Information Coefficient and Boruta methods were employed to extract the uncertainty index particularly correlated with BDI as an exogenous variable for forecasting. Then, we employ the K-Shape method to cluster exogenous variables and explore the combined sense of clustering. Finally, we utilize the Prophet model to forecast BDI in stages. It discusses the influence of exogenous variables and their cluster combinations on the forecasting effect individually and sequentially. Empirical results show that considering the two momentous events of the Financial Crisis and COVID-19 can remarkably improve the accuracy of BDI forecasting. In addition, the study of exogenous variable significance found that during the Financial Crisis, economic policy uncertainty in Europe and the Americas greatly impacted BDI forecasting. During COVID-19, global and developed economic policy uncertainty was noteworthy in the BDI forecasting. The comparative experimental results show the Prophet model has an exemplary forecasting result and strong robustness. It also performs excellently in model generalization and interpretability. This paper proposes a reliable and advanced algorithm for shipping freight rate index forecasting, which has noteworthy reference value for shipping market participants to make investment decisions and risk avoidance.

1. Introduction

The shipping industry is perceived as a substance global trade industry, with ships responsible for delivering over 80% of world trade (UNCTAD, 2022). It plays an essential role in the growth of the global economy and the stability of global supply chains. The international shipping market is mainly divided into four sub-markets: the dry bulk shipping market, the tanker shipping market, the container shipping market, and the particular vessel shipping market. As an essential component of the international maritime market, the dry bulk shipping market is subject to the impacts of the international economic and trade environment. Thus, it is widely recognized as a periodic market with high risk and volatility (Xu, Tao, Shu, & Wang, 2021).

As a representative variable of the shipping market, the freight rate not only reflects and regulates the state of the shipping market but also serves as an essential indicator influencing shipowners' investment decisions, balancing supply and demand, and securing cargo transportation (Xu & Yip, 2012; Schramm & Munim, 2021). The dry bulk freight rates are represented by the Baltic Dry Index (BDI), formerly the Baltic Freight Index (BFI), reflecting the spot market. The BDI is calculated by weighting spot freight rates on all significant routes worldwide, effectively reflecting the global dry bulk freight rates and the state of the

* Corresponding author.
E-mail addresses: wangwenyang@dlmu.edu.cn (W. Wang), henan@dlmu.edu.cn (N. He), chenmuxin2336@dlmu.edu.cn (M. Chen), jiapeng@dlmu.edu.cn (P. Jia).

https://doi.org/10.1016/j.eswa.2024.123451
Received 17 October 2023; Received in revised form 12 December 2023; Accepted 8 February 2024
Available online 14 February 2024

dry bulk market. Simultaneously, as a leading authoritative index reflecting international trade conditions, the BDI is widely regarded as an essential barometer of the shipping market boom, global economic performance, and international trade demand. The BDI offers dynamic information about international shipping and is often considered an influential warning indicator for economic crises. Therefore, accurate forecasting of the BDI not only assists shipping market participants, government administrators, and financial investors when making optimal decisions but also improves the efficiency of global economic activity. However, BDI is challenging to forecast. From the perspective of the data, the BDI is featured by non-linearity, non-stationarity, and high volatility. Its forecasting is affected not only by trend and seasonality but also by changes in supply and demand of the shipping market, which are essential influencing factors (Bai, Lam, & Jakher, 2021; Bildirici, Şahin Onat, & Ersin, 2023). From the view of the model, traditional time series forecasting models, such as the Autoregressive Integrated Moving Average Model (ARIMA), show defects like non-stationarity and non-linearity in BDI forecasting, leading to unsatisfactory forecasting results (Dai, Zeng, & Chen, 2016). Simple machine learning models, such as Artificial Neural Network (ANN), produce perfect nonlinear fits, but their network structures are unstable and have deficient interpretability (Zhang, Xue, & Stanley, 2018). In addition, as the external environment becomes increasingly complex, frequent wars and natural disasters pose high risks to the shipping market and cause new difficulties to BDI forecasting. It is, therefore, necessary to select an efficient and accurate model and consider the combined influence of inherent characteristics of the shipping market and the external factors to forecast BDI.

This paper proposes a BDI forecasting method that considers the impact of momentous and significant events. Firstly, the BDI sample set is divided into two periods based on two landmark momentous emergencies: the Global Financial Crisis in 2008 and the COVID-19 pandemic in 2019. The two periods are completely independent, and each period is divided into a training set and a test set according to a specific ratio, so setting the model parameters individually for one period to make a BDI forecasting will not impact the other period. Secondly, a significant event database is built, which consists of numerous indexes measuring world uncertainty events such as politics, war, economy, and climate change. Meanwhile, the uncertainty indexes are normalized to construct a standard database of factors affecting freight rate indexes. Then, the uncertainty indexes related to BDI are extracted from the significant events database to compose significant influencing factors clustered. Finally, a model considering the influence of multi-dimensional significant events is constructed to forecast the BDI.

Theoretically, we innovatively investigate the impact of multi-dimensional significant emergencies on freight rate index forecasting, providing a novel and practical methodology. Operationally, we establish a database of significant events, representing uncertain events in multiple areas. It is also applicable to other indexes forecasting studies. Simultaneously, the research on the impact of significant events on the freight rate index provides a new direction for risk prevention, shipping finance controlling and the investment management of shipping derivatives.

The rest of the paper is organized as follows. Section 2 reviews the literature related to the shipping market, particularly the BDI study. Section 3 delivers the model and methodology employed in the present paper. The empirical analysis and results are presented in Section 4. Section 5 proposes a robustness test of the model, and Section 6 concludes the study and offers the future outlook.

2. Literature review

The basis of this paper is the research on shipping freight rates, specifically the research on the BDI. First, this section begins with a review of the research on shipping freight rates, which is the groundwork. From the perspective of research objects, dry bulk freight rates, container freight rates, and tanker freight rates are widely and typically studied. From the outlook of research content, the studies focus on the volatility, forecasting, and influencing factors of freight rates. Secondly, this section shows an overview of the research literature on BDI forecasting. The research on the influencing factors of BDI and the application of the "decomposition-integration" idea form the content and methodologies of our study. Finally, this section summarizes the literature on the Prophet model. The development of shipping freight rates research is shown in Fig. 1.

2.1. Freight rates study

According to the segmentation of the shipping market, freight rates research involves dry bulk freight rates research, container freight rates research, and tanker freight rates research, where the specific perspectives include volatility, influencing factors, and forecasting of freight rates.

Numerous scholars have explored the non-stationarity, non-linearity, and seasonality of freight rates in the study of volatility. For dry bulk freight rates, Veenstra and Franses (1997), based on dry bulk freight rates samples, found that the freight itself is non-stationary, but there is a stable long-term relationship between the different freight series. Kavussanos and Alizadeh-M (2001) pointed out a significant deterministic seasonality in dry bulk freight rates, and the seasonality varies depending on the vessel's size and the transported commodity's properties. Jing, Marlow, and Hui (2008) studied the volatility characteristics of freight rates for different vessel sizes. They concluded that the external shocks to the market have distinct effects on the volatility of different vessel sizes. In the study of tanker freight rates, Kavussanos and Alizadeh-M (2002) confirmed the conclusion that Kavussanos and Alizadeh-M (2001) had applied equally to the tanker freight rates. Subsequently, Adland and Cullinane (2006) explored tanker freight rates' non-stationary and non-linear features. By extracting the constituent cycles, Siddiqui and Basu (2020) found that longer cycles contribute strongly and positively, while short and medium cycles tend to show weak adverse effects on respective freight rates. Yin and Shi (2018) discovered the seasonality on various container routes by studying the CCFI, filling the research gap on the volatility features of container freight rates. The studies mentioned above and provide a theoretical orientation for forecasting techniques considering freight rates' non-stationary, non-linear, and seasonal features.

In the study of influencing factors, several scholars explored the internal characteristics of freight rates. Veenstra and Franses (1997) found a stable long-term relationship between dry bulk freight rates series, but this relationship does not improve the accuracy of freight rates forecasting. Poblacion (2015), for the first time, incorporated seasonality into a factor model to analyze the stochastic behavior of Time Charter Equivalent (TCE) and World Scale (WS) prices and found that models allowing for stochastic seasonality outperform models with deterministic seasonality. In addition, more scholars focused on the micro and macro environmental factors affecting freight rates. Wilmsmeier and Hoffmann (2008) concluded that liner shipping freight rates are significantly correlated with liner shipping services and port infrastructure structure. Alizadeh and Talley (2011a,b) discovered that specific ship details, including the ship's deadweight, vessel age, shipping routes, and the length of the laycan period, are essential determinants of dry bulk freight rates. Adland, Cariou, and Wolff (2016) added the characteristic factors of charterers, shipowners, and their matches. In contrast to the previous studies, which utilized data as a proxy for market confidence, Bai, Lam, and Jakher (2021) utilized news archives directly to capture shipping market sentiment. They confirmed that the news sentiment index is an essential predictor of freight rates. In recent years, scholars have directed their attention to the effects of macro-environmental factors on freight rates. These factors include wars, conflicts, financial crises, geopolitical risks, economic policy uncertainties, and public health events (Klovland, 2002; Chen, Miao, Tian, Ding, & Li, 2017;

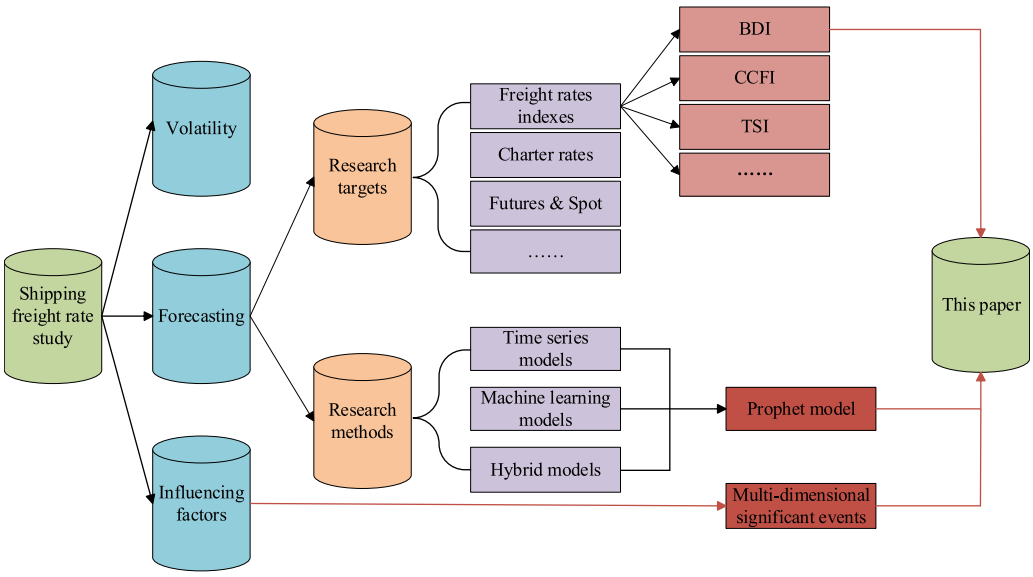

Fig. 1. Development network diagram of literature research (the abbreviations in the figure mean: CCFI-China Containerized Freight Index, TSI-Tianjin Shipping Index).

Drobetz, Gavriilidis, Krokida, & Tsouknidis, 2021; Khan, Su, Tao, & Umar, 2021; Gu & Liu, 2022; Rožić, Naletina, & Zając, 2022). As mentioned above, internal and external factors that have the potential to impact freight rates are increasingly being applied as exogenous variables in freight rates forecasting to improve accuracy.

In the study of forecasting methods, the usual forecasting objects are as follows: spot and forward freight rates (Batchelor, Alizadeh, & Visvikis, 2007), the Baltic Panamax Index (BPI) (Yang & Mehmed, 2019), the Shanghai Containerized Freight Index (SCFI) (Schramm & Munim, 2021), BDI (Katris & Kavussanos, 2021), the Tianjin Bulk Freight Index (TBI) (Gu & Liu, 2022), charter rates (Mo, Gao, Liu, Du, & Yuen, 2022), and the China Coastal Bulk (Coal) Freight Index (CBCFI) (Li et al., 2022). Traditional time series models are widely employed for forecasting, such as ARIMA, Generalized AutoRegressive Conditional Heteroskedasticity (GARCH), and Vector Autoregressive (VAR). Machine learning models are represented by Support Vector Regression (SVR) and ANN. As the features of the freight rates indexes are gradually being mined, it has been found that the combinatorial models have more satisfactory performance in forecasting. Kamal, Bae, Sunghyun, and Yun (2020) combined three deep learning models (Long Short Term Memory (LSTM), Recurrent Neural Network (RNN), and Gate Recurrent Unit (GRU)) to forecast the BDI and confirmed that the combinatorial forecasting technique outperforms ARIMA, RNN, LSTM, GRU, and Multi-Layer Perceptron (MLP). Chen, Liu, and Wang (2021) proposed a hybrid model consisting of grey wave forecasting and Empirical Mode Decomposition (EMD) based on the idea of "decomposition-reconstruction-integration", and the results showed that the hybrid model can improve the accuracy of CCFI forecasting. Hao, Yuan, Wu, Xu, and Li (2023) innovatively proposed a dynamic integrated forecasting method that integrates SVR, RVM, ANN, and LSTM to introduce metabolic mechanisms to improve BDI forecasting accuracy.

Current literature investigates the freight rates in the dry bulk, container, and tanker shipping markets, respectively, and selects representative freight rate index for attentive analysis. It not only explores the features of freight rates but also pays attention to the influencing factors and forecasting methods. Previous literature has explored freight rates' non-stationary, non-linear, and seasonal features in various sub-markets. It has combined them with micro and macro environmental factors as crucial indicators for freight rate forecasting. Additionally, forecasting models have undergone the development trajectory of econometric models, machine learning models, and combinatorial models. The above literature review indicates that the dry bulk market is frequently researched. Therefore, this paper examines the BDI, a representative index of the dry bulk market, and focuses on its forecasting methods.

2.2. *BDI forecasting*

Since the inception of the BFI in 1985, considerable researchers and scholars have conducted in-depth studies on the volatility and trend forecasting of the BFI or BDI. In terms of research perspective, some scholars conducted forecasting studies based on the characteristics of the BDI itself. Duru (2010) developed a fuzzy time series methodology to test the volatility features of the BDI to support short-term forecasting. Papailias, Thomakos, and Liu (2017) focused on BDI annual cyclicality and discovered that utilizing cyclical features in forecasting can improve performance. In order to better grasp the volatility features of BDI and improve the forecasting level, scholars have established comprehensive models by combining influencing factors. The selected influencing factors can be divided into regular factors, such as commodity prices with cyclical features. McPhail, Du, and Muhammad (2012) investigated the importance of crude oil prices in explaining the volatility of BDI. Gu, Chen, and Lien (2019) found volatility spillover effects between iron ore and BDI, where an increase in the spot price of iron ore pushes up the BDI. Pepur, Peronja, and Laća (2022) explored whether the S&P 500 stock index, the Shanghai Stock Exchange Composite (SSEC) index, 10-year bond yield, the Commodity Research Bureau (CRB) index, and West Texas Intermediate (WTI) Crude oil can impact the volatility of BDI. The Economic Policy Uncertainty (EPU) index, initially developed by Baker, Bloom, and Davis (2016), varies across countries. Subsequently, EPU has been employed in BDI studies as an essential indicator of economic uncertainty, e.g., Gu and Liu (2022) studied the impact of China's EPU on dry bulk freight rates; Gao, Zhao, and Zhang (2023) examined the linear and non-linear relationship between BDI and Global Economic Policy Uncertainty (GEPU). The second category includes sudden and random events, such as natural climate changes, geopolitical conflicts, financial crises, and public health securities. Michail and Melas (2020) quantified, for the first time, the relationship between the BDI and the number of people infected by COVID-19, i.e., a 1% increase in the number of cases is associated with a 0.03% decrease in the BDI. Bouri, Gupta, and Rossini (2022) investigated the impact of the El Niño-Southern Oscillation (ENSO) ocean climate index on BDI forecasting and

confirmed that models incorporating ENSO improve predictability. There have been fewer studies overall on the impact of significant events on the shipping market, and the existing literature mainly explores their impact on the volatility of the freight rates index. Rare studies have examined significant events as exogenous variables affecting BDI forecasting, and previous literature focused on only one significant event. We aim to fill this gap by using multi-dimensional indexes that can measure various uncertainty events for BDI forecasting and explore the key indexes that can enhance the accuracy of BDI forecasting to supply scientific references for investors and policymakers engaged in the shipping trade.

Regarding research methodology, Cullinake (1992) pioneered a forecasting methodology for the BFI index utilizing the ARIMA model. Subsequently, many scholars have researched the forecasting of BDI employing econometric and statistical models such as ARIMA, VAR, GARCH, and other related models. Veenstra and Franses (1997) employed cointegration and unit root tests to establish VAR model for forecasting the BDI. With the extensive application of big data and machine learning techniques, Duru, Bulut, and Yoshida (2012) utilized the Fuzzy-DELPHI (FD) method, and Şahin, Gürgen, Ünver, and Altin (2018) employed the ANN method to forecast BDI. Since then, more scholars have recognized that a single model alone cannot adequately extract the key features of a complex series. Therefore, some scholars have started integrating econometric and machine learning models to achieve accurate forecasts through time series data decomposition. Zeng and Qu (2014) conducted a study on the volatility of BDI using EMD. They decomposed the original BDI series into three distinct components: short-term changes, long-term trends, and external shocks. This method proved effective in revealing the features of the freight rates series. EMD was subsequently employed in combination with other models to forecast BDI. Zeng, Qu, Ng, and Zhao (2016) combined EMD with ANN to decompose the constituents obtained from EMD and model them separately. The results showed that the EMD-ANN method is superior to ANN and VAR methods, and their study offered an innovative and practical idea for dry bulk market analysis and forecasting. Based on EMD, Luo, Guo, Liu, and Zhang (2021) used the Ensemble Empirical Mode Decomposition (EEMD) to propose a hybrid model combining EEMD, ARIMA, and Taylor expansion. The results showed that the hybrid approach outperforms the benchmark utilized.

As shown in Table 1, in the research of BDI influencing factors, scholars have increasingly attached importance to the uncertainty indexes and momentous emergencies such as the COVID-19 pandemic. However, current literature concentrates on using uncertainty indexes to measure the economic domain while ignoring the domains of politics, war, and disease.

As illustrated in Table 2, models have evolved from simple econometric models to machine learning and deep learning models, and the idea of "decomposition-integration" has been increasingly applied to BDI forecasting. Multiple empirical results show that combinatorial models outperform single models in time series forecasting, which is becoming the mainstream direction of research (Zhang, Xue, & Stanley, 2018). By comparison, econometric models are computationally simple but unable to capture the non-linear features of the BDI. Machine learning models produce perfect non-linear fits. However, their structure is difficult to determine. Combinatorial models are computationally complex.

Table 2
Summary of literature related to BDI forecasting models.

Literatures	Models	Categories
Cullinake (1992)	ARIMA	Econometric Models
Veenstra and Franses (1997)	VAR	
Duru, Bulut, and Yoshida (2012)	FD	Machine Learning Models
Şahin, Gürgen, Ünver, and Altin (2018)	ANN	
Zeng and Qu (2014)	EMD	"Decomposition-Integration"
Zeng, Qu, Ng, and Zhao (2016)	EMD-ANN	
Luo, Guo, Liu, and Zhang (2021)	EEMD-ARIMA	

2.3. Prophet model

The Prophet model is a time series data forecasting method that blends the features of traditional time series forecasting and machine learning methods to achieve an optimal balance between interpretability, forecast accuracy, and automation (Taylor & Letham, 2018). Several studies have shown the Prophet model outperforms traditional forecasting models. Yenidoğan, Çayir, Kozan, Dağ, and Arslan (2018) compared the Prophet and ARIMA forecasting results for Bitcoin price. They concluded that the forecasting performance of the Prophet model is more reasonable than that of ARIMA. Satrio, Darmawan, Nadia, and Hanafiah (2021) also confirmed that the Prophet model is significantly sounder than ARIMA in forecasting the number of people infected by COVID-19 in Indonesia. Chaturvedi, Rajasekar, Natarajan, and McCullen (2022) verified that the Prophet model significantly outshines econometric models such as Seasonal Auto Regressive Integrated Moving Average (SARIMA), deep learning models such as LSTM RNN in forecasting the monthly total energy demand in India. Although the Prophet model has been widely employed, it has not yet been popularized in shipping finance. Through a study of financial time series, Yusof, Khalid, Hussain, and Shamsudin (2020) pointed out that the Prophet model has the advantages of efficiency and accuracy and is competitive in simulating actual market movements, with forecasting comparable to those of more sophisticated forecasting models. Saeed, Nguyen, Cullinane, Gekara, and Chhetri (2023) utilized the Prophet model for the first time for container freight rates forecasting by simulating the impact of a momentous event (the COVID-19 epidemic) using the "holiday" module of the Prophet model. The results showed that the Prophet model, with the effect of the momentous event, has better forecasting performance, which confirmed the advantages of the Prophet model in terms of interpretability. Unlike their studies, we employ the Prophet model for BDI forecasting and introduce the impact of the Financial Crisis and the COVID-19 epidemic in stages. To the authors' knowledge, this paper is the first BDI forecasting study using the Prophet model.

The primary advantages of the methodologies employed in this paper

Table 1
Summary of relevant literature on BDI influencing factors.

Literatures	Influencing Factors	Perspectives
Duru (2010)	Volatility Features of the BDI	Features Analysis of the BDI
Papailias, Thomakos, and Liu (2017)	Cyclical Features of the BDI	
McPhail, Du, and Muhammad (2012)	Price of Crude Oil	Cyclical Variables
Gu, Chen, and Lien (2019)	Price of Iron Ore	
Pepur, Peronja, and Laća (2022)	Stock Market Index	
Gu and Liu (2022)	China's EPU	Uncertainty Indexes
Gao, Zhao, and Zhang (2023)	GEPU	
Michail and Melas (2020)	COVID-19 Pandemic	Non-cyclical Variables
Bouri, Gupta, and Rossini (2022)	ENSO	

compared to previous literature on shipping freight rates indexes are as follows. (1) Expandability. Unlike the existing literature discussing the determinants of the BDI, we construct a multi-dimensional significant events variables database by extracting vital variables to support the study of the impact of specific events on the BDI. The forecasting object can be extended to other freight rate indexes in the shipping market. (2) Interpretability. Unlike employing the traditional time series forecasting models, machine learning models, and their combinatorial models, we utilize a single Prophet model to combine the intrinsic laws of the BDI with the external variables affecting the BDI to build a comprehensive forecasting model. This methodology can both capture the volatility features of the BDI and explore the mechanism of the external variables affecting the BDI. (3) Efficiency. The Prophet model, with fewer parameters, can achieve rapid parameter tuning. Unlike deep learning models, it runs faster and has more straightforward computation than combinatorial models. (4) Accuracy. According to our study, the Prophet model is a time series forecasting method with high accuracy. In addition, the model developed in this paper supports the identification of the location of BDI mutations and outliers, which offers a warning role for investors, operators, and managers, thus enabling them to make scientific decisions.

3. Model interpretation

Fig. 2 illustrates the models and methods employed in this study. For uncertainty indexes screening, firstly, the Maximal Information Coefficient (MIC) and Boruta algorithm are employed to screen significant uncertainty indexes impacting the BDI. Secondly, the K-Shape technique clusters the significant uncertainty indexes mentioned above. For BDI forecasting, firstly, the critical components of the BDI (trend, seasonality, and shocks from momentous emergencies) are decomposed and integrated using the Prophet model, which is an integral part of the forecasting model. Secondly, essential uncertainty indexes and their clustering combinations are substituted into the model to explore significant emergencies' impact on BDI forecasting. The feature screening, cluster analysis, and forecasting method will be described below.

3.1. Features screening

This paper employs numerous uncertainty indexes to establish a significant emergency database. Due to the numerous uncertainty indexes involved, the "MIC-Boruta" two-layer feature screening technique was utilized to minimize redundant variables and enhance model forecasting accuracy. Uncertainty indexes with a high degree of relevance to BDI and a significant impact on BDI forecasting have been screened out from the database of significant emergencies. MIC, which is widely employed for feature selection, has two properties: universality and fairness (Reshef et al., 2011). Compared to the Pearson correlation coefficient, MIC is more robust, capturing a broader spectrum of complex correlations and not limited to specific function types (Lin, Lin, & Gu, 2022). Unlike the existing feature selection methods, the basic idea of Boruta is to filter out all the sets of features correlated with the dependent variable. Previous research indicates that Boruta outperforms other Random Forest-based feature selection methods (Speiser, Miller, Tooze, & Ip, 2019; Nemani et al., 2022), and the selected feature variables significantly enhance forecasting performance.

3.1.1. MIC

Definition 1. *Given two random variables* $\boldsymbol{X}, \boldsymbol{Y}$ *in the data set,* $\boldsymbol{X} = \{x_1, \ldots, x_n\}, \boldsymbol{Y} = \{y_1, \ldots, y_n\}$, n *is the number of samples. The mutual information between* $\boldsymbol{X}$ *and* $\boldsymbol{Y}$ *is as Eq.* (1).

$$I(\boldsymbol{X};\boldsymbol{Y}) = \int_{\boldsymbol{Y}}\int_{\boldsymbol{X}} f(\boldsymbol{X},\boldsymbol{Y})\log_2\frac{f(\boldsymbol{X},\boldsymbol{Y})}{f(\boldsymbol{X})f(\boldsymbol{Y})}d\boldsymbol{X}d\boldsymbol{Y} \tag{1}$$

where $f(\boldsymbol{X};\boldsymbol{Y})$ is the joint probability density function, $f(\boldsymbol{X})$ and $f(\boldsymbol{Y})$ denote the marginal probability density of $\boldsymbol{X}$ and $\boldsymbol{Y}$, respectively. Based on mutual information, Reshef et al. (2011) proposed a new algorithm to measure the strength of correlation between two variables-MIC. MIC can find the degree of linear and non-linear correlation between the input variable $\boldsymbol{X}$ to be selected and the output variable $\boldsymbol{Y}$ to the maximum extent possible. The calculation of MIC is as Eq. (2).

$$\mathrm{MIC}(\boldsymbol{X};\boldsymbol{Y}) = \max_{a\times b<B}\frac{I(\boldsymbol{X};\boldsymbol{Y})}{\log_2\min(a,b)} \tag{2}$$

where B is the maximum upper limit on the number of $a \times b$ grids to be constructed, representing the correlation function of sample size. The stronger the correlation between $\boldsymbol{X}$ and $\boldsymbol{Y}$, the larger the value of $\mathrm{MIC}(\boldsymbol{X};\boldsymbol{Y})$, which tends to be 1. Conversely, if the two are independent of each other, then $\mathrm{MIC}(\boldsymbol{X};\boldsymbol{Y})$ tends to be 0.

3.1.2. Boruta algorithm

After the initial screening using MIC, redundant variables and variables with weak correlations still lead to long run times and poor generalization of the forecasting model. To address this issue, a Boruta-based variable selection algorithm was employed for further variable screening.

Boruta algorithm is a feature screening method whose theoretical idea originates from random forests. The process involves adding more randomness to the system to screen features (Kursa & Rudnicki, 2010). The basic idea is to utilize an iterative method during feature screening

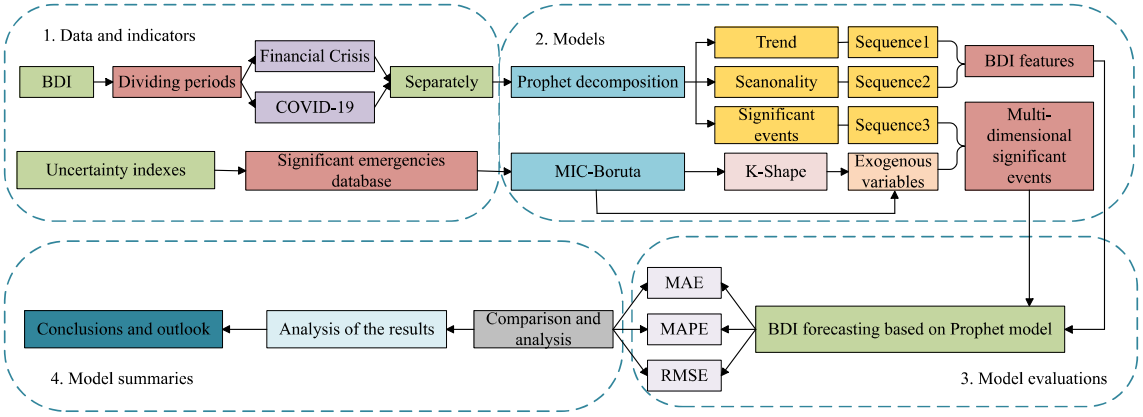

Fig. 2. Flowchart of the model (the abbreviations in the figure mean: MAE-Mean Absolute Error, MAPE-Mean Absolute Percentage Error, RMSE-Root Mean Square Error).

that involves the removal of low-correlation features, retention of high-correlation features, and filtering out the set of features with high correlation to the dependent variables based on Mean Decrease Accuracy. The steps for feature screening are illustrated in Algorithm 1: Features Screening.

Algorithm 1: Features Screening

Input: The variable to be predicted y and characteristic variables x_i obtained from the initial screening of Eq. (2).
for $i = 1, 2, ..., n$ do
Step 1: Shadow features are obtained by adding randomness to all features of the original datasets;
Step 2: The original dataset is merged with the shadow feature set to create an extended dataset;
Step 3: Utilize a random forest classifier to assign a feature score Z_{sore} to the original and shadow features. The higher the value of Z_{sore}, the more influential the feature is;
Step 4: Calculate the whole features' importance. If a feature's importance is higher than the maximum importance of all shadow features, the feature is considered essential and accepted.
End
Identify rejected or accepted features.
Output: Accepted features.

3.2. K-Shape Time series cluster analysis

K-Shape is a clustering algorithm that preserves the native shape of the time series (Paparrizos & Gravano, 2015). The K-means has often been employed for time series clustering analysis. However, the K-means utilizes the Euclidean Distance to measure the similarity between different time series and thus performs poorly for time series with significant volatility (Hartigan & Wong, 1979; Cheng, Chen, & Jian, 2016; Wu, Mu, Deng, & Li, 2022). The K-Shape algorithm utilizes the Normalized Cross-Correlation Coefficient (NCCc) as a distance metric and assigns time series by calculating the clustering center of mass. It can effectively summarize a set of time series based on only one sequence and extract the most representative shapes from the underlying data to effectively cluster time series (Yang et al., 2017; Fahiman, Erfani, Rajasegarar, Palaniswami, & Leckie, 2017). Therefore, we employ K-Shape to cluster uncertainty indexes.

Definition 2. *Define* $CC_w(\boldsymbol{X}, \boldsymbol{Y}) = R_{w-m}(\boldsymbol{X}, \boldsymbol{Y}),\ w \in \{1, 2, ..., 2m-1\}$ *as the cross-correlation measure of the time series* $\boldsymbol{X}$ *and* $\boldsymbol{Y}$ *.* $R_{w-m}(\boldsymbol{X}, \boldsymbol{Y})$ *is*:

$$R_{w-m}(\boldsymbol{X}, \boldsymbol{Y}) = \begin{cases} \sum_{l=1}^{2m-w} \boldsymbol{X}_l + (w-m)\cdot \boldsymbol{Y}_l, w - m \geqslant 0 \\ R_{-(w-m)}(\boldsymbol{Y}, \boldsymbol{X}), w - m < 0 \end{cases} \tag{3}$$

where $w - m$ is the drift correction factor and $w - m \in [-m, m]$, $\boldsymbol{X}$ and $\boldsymbol{Y}$ are the time series of length m.

In order to investigate the combinatorial effect between uncertainty indexes and to explore the impact of the clustering results on BDI forecasting, this paper utilizes the K-Shape method, combined with the Elbow Method, to perform clustering operations on the screened feature variables. The Elbow Method is an effective method for determining the optimal number of clusters, and its core metric is the Sum of the Squared Errors (SSE) (Lücke & Forster, 2019). SSE is shown in Eq. (4).

$$SSE = \sum_{i=1}^{k} \sum_{p \in C_i} (p - m_i)^2 \tag{4}$$

where C_i is the i th cluster, p is a sample point in C_i, and m_i is the center of mass of C_i (the mean of all samples in C_i). SSE is the clustering error for all samples and represents how well the clustering works. According to Definition 2, the clustering step is shown in **Algorithm 2**: Cluster Analysis Algorithm.

Algorithm 2: Cluster Analysis Algorithm

Input: Given n time series data with length of m, $\boldsymbol{X}_i = \{x_{i1}, ..., x_{im}\}$.
for $i = 1, 2, \cdots, n$ do
Step 1: Measure the distance between two time series $\boldsymbol{X}_i$ and $\boldsymbol{X}_j$ according to
$SBD(\boldsymbol{X}_i, \boldsymbol{X}_j) = 1 - \max_w \left(\frac{CC_w(\boldsymbol{X}_i, \boldsymbol{X}_j)}{\sqrt{\sum_{i=1}^{m} \boldsymbol{X}_i \cdot \sum_{j=1}^{m} \boldsymbol{X}_j}} \right)$;
Step 2: Determine the optimal number of clusters by Elbow Method;
Step 3: Calculate the center of mass based on $\boldsymbol{\mu}_k^* = \underset{\boldsymbol{\mu}_k}{\operatorname{argmax}} \frac{\boldsymbol{\mu}_k^T \left(\boldsymbol{I} - \frac{1}{m}\boldsymbol{O}\right)^T \sum_{\boldsymbol{\mu}_k \in \boldsymbol{P}_k} (\boldsymbol{\mu}_i \boldsymbol{\mu}_i^T)^2 \left(\boldsymbol{I} - \frac{1}{m}\boldsymbol{O}\right)^T \boldsymbol{\mu}_k}{\boldsymbol{\mu}_k^T \boldsymbol{\mu}_k}$ and perform shape extraction of the time series.
End
Determine the clustering results.
Output: Clustering results.

In step 1, $SBD(\boldsymbol{X}_i, \boldsymbol{X}_j)$ takes values from 0 to 2. The similarity between the two time series increases as $SBD(\boldsymbol{X}_i, \boldsymbol{X}_j)$ decreases. In step 3, the maximum value $\boldsymbol{\mu}_k^*$ indicates the squared similarity of all other time series, $\boldsymbol{P}_k$ is the kth class of aggregated data sets, $\boldsymbol{I}$ is the unit matrix and $\boldsymbol{O}$ is a symmetric matrix whose elements are all one.

3.3. Prophet model

The Prophet model is a data forecasting algorithm for time series. Its main principle is to mine the features of the time series and decompose them into four components: trend, seasonality, holidays, and residuals (Taylor & Letham, 2018). Compared to other models, it has the following advantages in forecasting BDI: (1) Powerful and precise fitting. It can fit the trend, seasonality, and impact of momentous events of the BDI, which helps to study the intrinsic patterns and external impacts of the BDI. (2) Less and sparse parameter space. The number of parameters of the Prophet model is much smaller than that of deep schemes, which are challenging to overfit and converge rapidly. (3) Understood and accessible interpretation. Powerful visual analysis aids are provided to analyze the contribution of trend, seasonality, and momentous events in the BDI forecast. Since BDI is characterized by nonlinearity, non-stationarity, and volatility, direct forecasting using general models is ineffective, so we adopt the Prophet model to decompose the BDI series into simple ones. Eq. (5) explains the Prophet model.

$$y(t) = g(t) + s(t) + h(t) + \varepsilon_t \tag{5}$$

where t denotes time, $g(t)$ is a trend term indicating the trend of the time series, $s(t)$ denotes a period term (seasonal term), $h(t)$ denotes a holiday term (event), and ε_t denotes an error term (residual term).

3.3.1. Trend term

Trend analysis identifies long-term trends in time-series data, essential for forecasting future movements. Decomposing the BDI shows that the BDI exhibits a steady upward or steady downward or leveling trend over an extended period.

The trend terms of the Prophet model are categorized into logistic regression functions and segmented linear functions. The trend term based on logistic regression can be expressed as:

$$g(t) = \frac{C}{1 + \exp(-k(t - m))} \tag{6}$$

where C is the carrying capacity, k is the growth rate, and m is the offset

parameter.

The trend term based on segmented linearity can be expressed as:

$$g(t) = \left[k + \boldsymbol{a}(t)^T\boldsymbol{\delta}\right]t + \left[m + \boldsymbol{a}(t)^T\boldsymbol{\gamma}\right] \tag{7}$$

where $\boldsymbol{\delta}$ represents the amount of change in the growth rate, consisting of the change point s_j and the growth rate δ_j $(j = 1, 2, ..., m)$ at the change point; $\boldsymbol{\delta} \in \mathbb{R}^b$, $\delta_j \sim Laplace(0, \pi)$; $\boldsymbol{\gamma} = \left\{\gamma_1, ..., \gamma_j\right\}$, $\gamma_j = -s_j\delta_j$, denotes the offset correction term, which ensures that the function is continuous; $\boldsymbol{a}(t) = \left\{a_1(t), ..., a_j(t)\right\}$.

3.3.2. Seasonal term

Seasonality is a cyclical variation that keeps recurring in the same time cycle. The seasonality of the BDI is mainly due to the differences in shipping costs and seaworthiness of ships in different seasons, as well as the seasonality of the demand for dry bulk cargoes, such as coal and grain. The purpose of analyzing the seasonality is to isolate the seasonality from the time series and analyze the seasonality pattern in the BDI separately. The Prophet utilizes the Fourier series for cycle modeling:

$$s(t) = \sum_{n=1}^{N}\left(a_n\cos\left(\frac{2\pi nt}{P}\right) + b_n\cos\left(\frac{2\pi nt}{P}\right)\right) \tag{8}$$

where $s(t)$ is the standard discrete Fourier series, N denotes the total number of cycles, P represents the period, which can be set to be yearly, weekly and hourly as a cycle, a_n and b_n are parameters.

3.3.3. Holiday term

The holiday term in the Prophet is defined as:

$$h(t) = \boldsymbol{Z}(t)\boldsymbol{\kappa} \tag{9a}$$

$$\boldsymbol{Z}(t) = [\mathbf{1}(t \in D_1), ..., \mathbf{1}(t \in D_L)] \tag{9b}$$

$$\boldsymbol{\kappa} = (\kappa_1, ..., \kappa_L)^T, \kappa_i \sim N(0, v^2), i = 1, 2, ..., L \tag{9c}$$

where D_i denotes the duration of the holiday; κ_i denotes the extent of the holiday's impact; L is the number of holidays; v is the size of the holiday, we set the value of $v = 10$ (we tried to test the parameter estimation of v for a better result, but $v = 10$ for both periods is optimal). In this paper, the holiday term is set by adding key time points to simulate the impact of two momentous emergencies, the Financial Crisis and the COVID-19 epidemic, on the BDI.

Overall, using the Prophet model to forecast the BDI, on the one hand, the trend term and seasonal term can more accurately capture the intrinsic pattern of the BDI, and on the other hand, the holiday term is conducive to quantifying the impact of momentous events on BDI. Meanwhile, since the Prophet model decomposes the BDI and forecasts only the decomposed subsequences first, this will improve the forecasting effect.

3.4. Criteria for forecasting performance

In order to compare the forecasting performance of different models, the loss function must be chosen for statistical tests. In this paper, three standard loss functions are employed: MAE, MAPE, and RMSE (Zhang, Cheng, Zhang, Wang, & Wang, 2023; Wang, Niu, Zhang, Liu, & Huang, 2023; Li, Zhang, Zhang, & Wang, 2024). MAE can avoid canceling out each other's errors and, therefore, can mathematically reflect the magnitude of the actual prediction error; MAPE is a statistical indicator label commonly utilized to calculate the forecast accuracy of a time series. It is sensitive to relative error and does not change due to the global scaling of the target variable; RMSE measures the deviation of the predicted value from the true value and is more sensitive to outliers in the data. Using multiple indicators to evaluate the forecasting performance of each model can more comprehensively and objectively reflect the strengths and weaknesses of the model and avoid the model selection bias caused by a single evaluation indicator. The MAE, MAPE, and RMSE evaluation indicators have the following definitions:

$$\text{MAE} = \frac{1}{n}\sum_{i=1}^{n}|\widehat{y}_i - y_i| \tag{10a}$$

$$\text{MAPE} = \frac{1}{n}\sum_{i=1}^{n}\left|\frac{\widehat{y}_i - y_i}{y_i}\right| \tag{10b}$$

$$\text{RMSE} = \sqrt{\frac{1}{n}\sum_{i=1}^{n}(\widehat{y}_i - y_i)^2} \tag{10c}$$

where y_i and $\widehat{y}_i$ are the actual and predicted values at moment i, n is the sample size of the test set. The smaller values of the metrics indicate more acceptable model forecasting performance.

4. Empirical analysis

4.1. Data description

4.1.1. BDI

In this paper, BDI is selected as the forecasting object, which is collected from the Clarkson Sin database. Considering the availability of data related to uncertainty indexes, the sample is set as monthly data from November 2001 to December 2022.

As shown in Fig. 3, in 2008, the BDI reached a record high, leading to a significant increase in shipping investment. However, the shipping market was severely affected by the Financial Crisis, resulting in a plummet in the BDI. This downturn and depression persisted until 2012. Subsequently, the shipping market recovered slowly, but the outbreak of COVID-19 curtailed its upward trend. As viewed, the Financial Crisis and COVID-19 have caused unusual volatility in the BDI, but their specific impacts need to be further studied.

Besides, the trend of BDI shows prominent cyclical characteristics. From 2001 to 2022, it has gone through 6 complete cycles (as shown by the dotted line in Fig. 3). The starting point of the six cycles is November 2001, August 2005, December 2008, February 2012, February 2016, and January 2020, with an average duration of about 1288.5 days (42.3 months) per cycle.

Multiple literatures have divided the sample into different periods for separate studies. Liu, Li, Sun, Yu, and Gao (2022) divided the sample set into the Financial Crisis period and the recent shipping market period, respectively, to conduct BDI forecasting studies and verify the robustness of the forecasting models. Zhao, He, Lu, Han, Ding, and Peng (2022) divided the sample set according to urban closure policies due to the epidemic to research the impact of COVID-19 on maritime transportation.

Based on historical literature and expanding on them, we consider the effects of the Financial Crisis and COVID-19 using February 2012 as the cut-off point and dividing the sample into two periods. The Period I ranged from November 2011 to January 2012 and was primarily influenced by the Financial Crisis. The Period II ranged from February 2012 to December 2022 and was mainly affected by the COVID-19 epidemic. We validate the statistical necessity of dividing the two periods using the Mann-Whitney U statistical test (Mann & Whitney, 1947; Wilcoxon, 1992). The results show that $stat = 13879.000$, $p = 0.000$, the two periods belong to different distributions, and the division of periods is statistically significant. In addition, we tried to change the starting and cut-off points, but none of the results were as significant as the two periods utilized in this paper. The density histogram of BDI for the two periods is shown in Fig. 4.

Both periods are divided into training and test sets according to the ratio of 80%-20%, for Period I, the training sample is from 2001-11 to

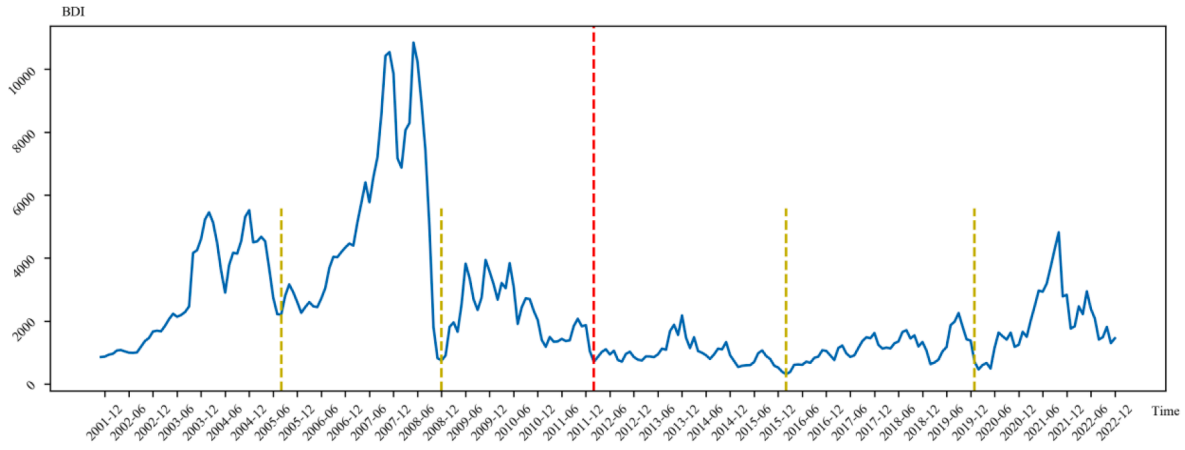

Fig. 3. BDI trends from November 2001 to December 2022.

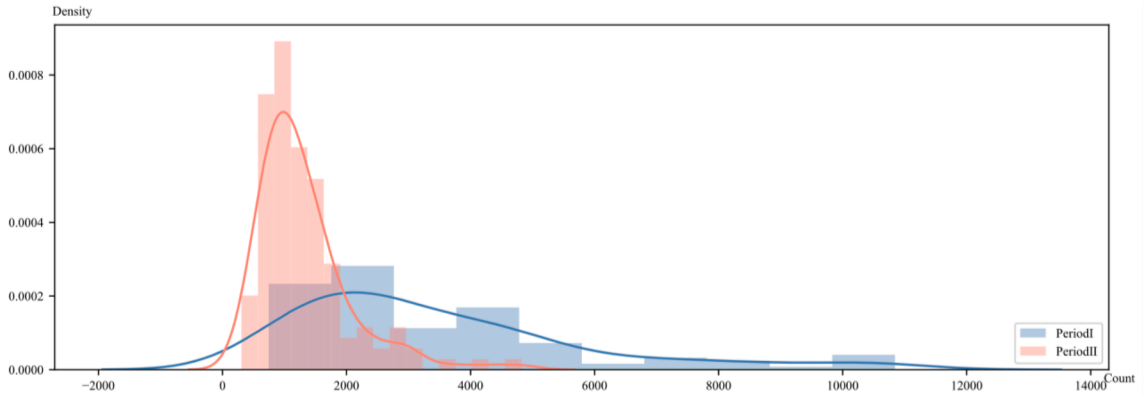

Fig. 4. Density histogram of BDI in two periods.

Table 3
Descriptive statistics of the samples.

Periods	Mean	Median	Minimum	Maximum	Standard deviation	Skewness	Kurtosis
Period I	3459.21	2719.45	743.00	10843.65	2325.26	1.38	1.62
Period II	1309.56	1123.13	306.90	4819.95	749.09	1.96	5.14

2010–01, and the test sample is from 2010-02 to 2012–01, while for Period II, the training sample is from 2012-02 to 2020–09, and the test sample is from 2020-10 to 2022–12. Table 3 shows the statistical information of the two periods.

4.1.2. Significant emergency events database

The primary emergency database comprises numerous uncertainty indexes from the database constructed by Baker, Bloom, and Davis (2016). Based on data availability and completeness principles, 377 uncertainty indexes were finally selected as relevant indicators for Period I and 445 uncertainty indexes for Period II. Subsequently, these indexes will be screened.

4.2. Screening of uncertainty indexes

In order to reduce the dimensional influence of the data, normalization was performed using the Min-Max normalization method, as shown in Eq. (11).

$$\widehat{X} = \frac{X - X_{\min}}{X_{\max} - X_{\min}} \tag{11}$$

Algorithm 1 was utilized to determine the 10 uncertainty indexes that exhibited the higher correlation with the BDI in both periods, as illustrated in Table 4 and Table 5. In Period I, the BDI boasts a stronger correlation with each country's economic and financial market fluctuations. However, the BDI in Period II is influenced by uncertain events such as politics, war, climate, and disease, in addition to the economic and financial market fluctuations mentioned above. The indexes screened at the two periods are distinct, which is mainly due to differences in the degree of response to shocks in each country.

For the countries we screened, we tried to interpret them in an economic sense, especially their practical correlation with the shipping industry (not just the BDI). As can be seen from Table 6, the vast majority are developed countries, and only Turkey, Chile, and China are developing countries. Moreover, most of countries above are closely linked to the shipping industry or commodity trade.

4.3. K-Shape-based Cluster analysis

In order to explore the impact of the combination of uncertainty indexes on BDI forecasting, we perform a K-Shape time series clustering analysis on the uncertainty indexes of the two periods separately to discover the potential cluster structure. The clustering results are added

Table 4
Definition and interpretation of relevant variables (Period I).

Variables (x_{ij}) [a]	Definition (abbreviation)	Policy types	Country/region	Correlation
x_{10}	Economic Policy Uncertainty of UK (EPUK)	Economic policy	UK	0.54
x_{11}	Economic Policy Uncertainty of Canada (EPUC)	Economic policy	Canada	0.51
x_{12}	Economic Policy Uncertainty of Australia (EPUA)	Economic policy	Australia	0.51
x_{13}	Economic Policy Uncertainty of Japan (EPUJ)	Monetary policy	Japan	0.49
x_{14}	Global Economic Policy Uncertainty Based on Purchasing Power Parity (GEPU)	Economic policy	Globe	0.48
x_{15}	American Financial Regulatory Policy Uncertainty (AFR)	Financial regulatory policy	USA	0.48
x_{16}	Economic Policy Uncertainty of Ireland (EPUI)	Economic policy	Ireland	0.48
x_{17}	Stock Market Volatility Tracker of America Based on Macroeconomic Policies (AM-EMV)	Macro-economy/Stock market	USA	0.46
x_{18}	Economic Policy Uncertainty of Spain (EPUS)	Economic policy	Spain	0.45
x_{19}	Economic Policy Uncertainty of Chile (EPUC*)	Economic policy	Chile	0.42

[a] Note: subscripts *ij* in each case refer to the period (*i*) and the order of the selected variable (*j*), as is Table 5.

Table 5
Definition and interpretation of relevant variables (Period II).

Variables (x_{ij})	Definition (abbreviation)	Policy types	Country/region	Correlation
x_{20}	Geographical Political Risk index (Terrorism) (GPRT)	Geopolitical event	Globe	0.48
x_{21}	Economic Policy Uncertainty of China (EPUC**)	Economic policy	China	0.48
x_{22}	Tax Policy Uncertainty of Greece (EPUGT)	Tax policy	Greece	0.45
x_{23}	Stock Market Volatility Tracker of America Based on Infectious Policies (AI-EMV)	Infectious diseases/ Stock market	USA	0.42
x_{24}	Global Economic Policy Uncertainty Based on Purchasing Power Parity (GEPU)	Economic policy	Globe	0.41
x_{25}	Economic Policy Uncertainty of Singapore (EPUS*)	Economic policy	Singapore	0.41
x_{26}	World Uncertainty Index of Turkey (WUI-TUR)	Uncertain event	Turkey	0.41
x_{27}	Tax Policy Uncertainty of America (EPUAT)	Tax policy	USA	0.39
x_{28}	Economic Policy Uncertainty of Canada (EPUC)	Economic policy	Canada	0.39
x_{29}	Climate Policy Uncertainty (CPU)	Climate policy	Globe [a]	0.39

[a] Note: global climate policy risk can be represented by the CPU index for America (Guo, Long, & Luo, 2022).

Table 6
The labels of the countries.

Countries	Labels
UK	"Developed country"; "Maritime Empire"; "Represented by the shipbuilding industry".
Canada	"Developed country".
Australia	"Developed country"; "The Country on a Mine Train"; "The world's fourth largest exporter of agricultural products and the world's largest exporter of a wide range of minerals".
Japan	"Developed country"; "Large fleet size".
USA	"Developed country"; "One of the countries with the largest number of maritime companies and the largest number of ships in the world".
Ireland	"Developed country".
Spain	"Developed country"; "Production and export of energy products, mainly oil and gas".
Chile	"Developing country"; "One of the world's leading producers of copper resources".
China	"Developing country"; "A major maritime nation, also a major shipping and shipbuilding nation".
Greece	"Developed country"; "World's largest shipping nation".
Singapore	"Developed country"; "The international shipping center with the strongest comprehensive strength in the world".
Turkey	"Developing country"; "The Mediterranean region, where Turkey is located, is precisely one of the busiest maritime regions in the world, accounting for approximately 25% of the world's maritime shipping".

to the forecasting model, combining multiple variables to improve its forecasting performance.

4.3.1. *Clustering results for Period I*

According to **Algorithm 2**, the optimal number of clusters for the 10 uncertainty indexes of Period I was determined to be $k = 3$. The final clustering results are shown in Fig. 5. The 10 variables in Period I are divided into 3 groups, as presented in Table 7.

P1_C1 includes the economic policy uncertainty of Japan, the UK, Canada, Australia, Ireland, and Global. Each country's economic policy uncertainty index is constructed using relevant newspaper information. The GEPU is calculated as the GDP-weighted average of the EPU indexes for 21 countries.

P1_C2 contains the economic policy uncertainty of Chile and Spain, which share the official Spanish language.

P1_C3 refers to policy uncertainty in North America, specifically in America, encompassing AFR and AM-EMV. Both indexes are constructed based on information from American newspapers, and AFR includes keywords such as bank regulation and financial reform. The American stock market volatility tracker is constructed based on the share of EMV articles discussing issues related to macroeconomic policy and captures American equity market volatility.

4.3.2. *Clustering results for Period II*

The optimal number of clusters for the 10 uncertainty indexes of Period II was determined to be $k = 5$. The final clustering results are shown in Fig. 6. The 10 variables in the Period II are categorized into 5 categories, as demonstrated in Table 8.

P2_C1 represents North American national policy uncertainty, which primarily refers to American financial market uncertainty, including AI-EMV and AEPUT. It can represent American financial market volatility. Among them, the American stock market volatility tracker considers the stock market volatility of contagious diseases, reflecting the response of the American stock market.

P2_C2 represents global climate policy uncertainty, which considers climate conditions such as global warming and greenhouse gases, as well

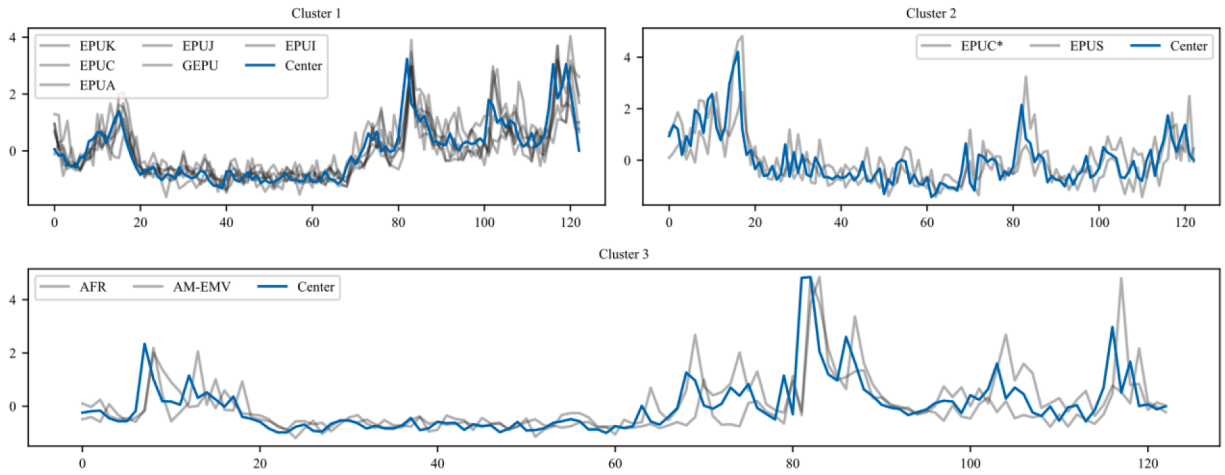

Fig. 5. Clustering results (Period I).

Table 7
Feature clustering results (Period I).

Categories	Features	Categories	Features
P1_C1	EPUJ (x_{13})	P1_C2	EPUC* (x_{19})
	EPUK (x_{10})		EPUS (x_{18})
	EPUC (x_{11})	P1_C3	AFR (x_{15})
	EPUA (x_{12})		
	EPUI (x_{16})		AM-EMV (x_{17})
	GEPU (x_{14})		

as related regulations and policies.

P2_C3 represents various uncertain events, including terrorist acts, wars, and politics.

P2_C4 represents Greece's tax policy uncertainty, which covers keywords such as tax and consumption tax.

P2_C5 includes the economic policy uncertainty of China, Singapore, Canada, and Global. Each country's economic policy uncertainty index is constructed using relevant newspaper information. The GEPU is calculated as the GDP-weighted average of the EPU indexes for 21 countries.

After clustering the uncertainty indexes of Period I and II using the K-Shape algorithm, the 10 uncertainty indexes of Period I were categorized into 3 categories, and the 10 uncertainty indexes of Period II were categorized into 5 categories based on the regions and meanings represented by the indexes. In terms of meaning, the clustering combinations represent uncertain economic, tax, climate, war, and disease events. Different combinations represent different meanings, which is the point of using the clustering algorithm in the article.

4.4. Prophet model application

4.4.1. Basic parameters

In this paper, a Prophet model for BDI forecasting was built based on the Python Prophet package (Taylor & Letham, 2018). Three fundamental parameters, growth trend flexibility (changepoint_prior_scale), changepoint selection range (changepoint_range), and intensity of seasonality (seasonality_prior_scale), were determined using the Grid

Table 8
Feature clustering results (Period II).

Categories	Features
P2_C1	AI-EMV (x_{23})
	AEPUT (x_{27})
P2_C2	CPU (x_{29})
P2_C3	GPR (x_{20})
	WUI-TUR (x_{26})
P2_C4	EPUGT (x_{22})
P2_C5	EPUC** (x_{21})
	GEPU (x_{24})
	EPUS* (x_{25})
	EPUC (x_{28})

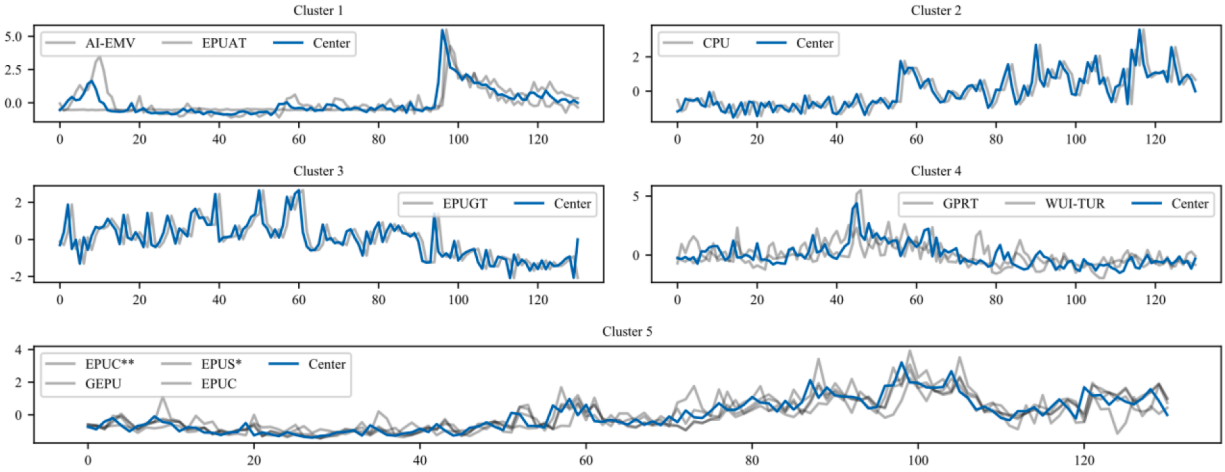

Fig. 6. Clustering results (Period II).

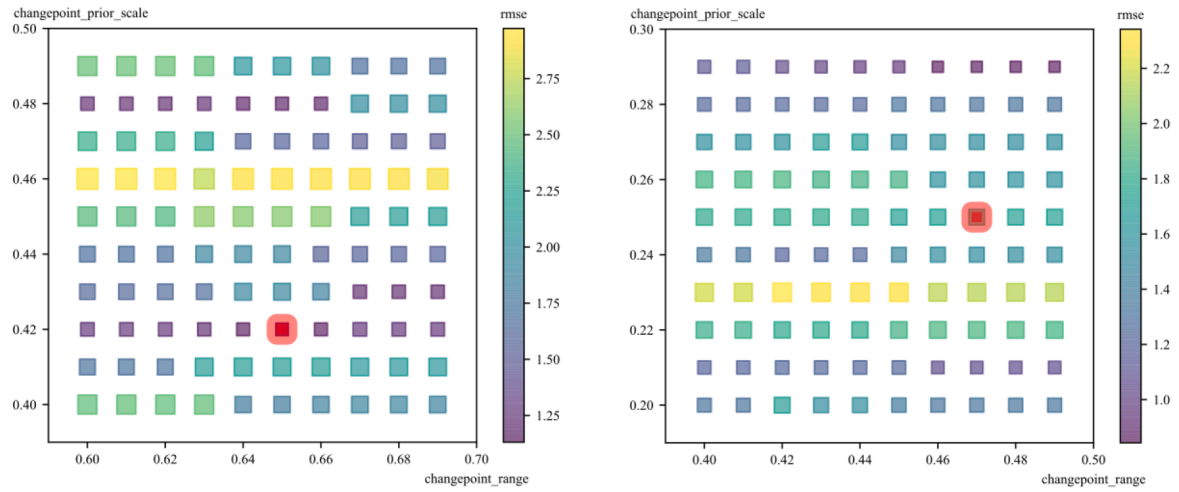

(a) (b)

Fig. 7. (a) Grid Search results of Period I; (b) Grid Search results of Period II (red is best).

Search method. We utilize rmse (see Eq. (10c)) to evaluate the performance of the model when parameters change. The steps are shown below.

Step 1: Initialization of the search range. Set the changepoint_prior_scale and the changepoint_range range at (0,1], with a step of 0.1. And the seasonality_prior_scale constantly searches from [0.1, 0.5, 1, 5, 10, 15, 20].

Step 2: Determination of the optimal subrange. After step 1, for Period I, the range of changepoint_prior_scale can be accurate to [0.40, 0.50] and the changepoint_range is [0.60, 0.70]; for Period II, the range of changepoint_prior_scale can be accurate to [0.20, 0.30], and the changepoint_range is [0.40, 0.50].

Step 3: Adjusting the search step size. Set the search step to 0.01 and perform another search for the two parameters mentioned in step 2.

Step 4: Determination of optimal parameter values. Theoretically, the rmse is computed from the training set, and the determined parameters are optimal when the rmse is minimum, but to prevent overfitting, we chose the most appropriate combination of parameters, the results are shown in Fig. 7 (with seasonality_prior_scale = 0.5).

Without considering the holiday term, the optimal parameter settings for the two-period model were determined, as shown in Table 9 below.

4.4.2. Holiday (event) parameterization

Considering the impact of the Financial Crisis and the COVID-19 epidemic, the $h(t)$ module in the Prophet model is utilized to set up the critical time nodes of the Financial Crisis and the COVID-19 epidemic to realize the modeling analysis of momentous events. The settings of Period I and Period II holidays (events) are shown in Table 10.

4.4.3. Forecasting results for Period I

The BDI is forecasted with the same length as the testing set in a one-step-ahead method, so as Period II. The forecasting results are shown in Fig. 8 and Fig. 9. When the impact of the Financial Crisis is added to the model, the annual seasonal subseries obtained from the decomposition changes significantly, and the out-of-sample forecasting ability improves, mainly in the period from July 2010 to March 2012 (shaded). In 2010, although the global economy had begun to recover from the Financial Crisis, the ensuing European Debt Crisis led to a resurgence of market volatility due to the turmoil, debt crisis, and recession.

In order to further study the degree and mechanism of influence of more uncertainty indexes on BDI, we added the uncertainty indexes and their clustering combinations into the model separately to construct the Prophet model considering uncertainty indexes. The out-of-sample validation results are shown in Table 11 (bolding is best, the same below). Compared with the original Prophet model, the predictive effect of the model adding the effect of the Financial Crisis is significantly

Table 9
Model parameterization.

Period I	Parameters	Set value	Interpretation
	growth	linear	Linear growth trend.
	seasonality	yearly	Annual seasonality.
	mcmc_samples [a]	20,000	The MCMC sampling times are 20000.
	changepoint_prior_scale	0.42	The intensity of the growth trend is 0.42.
	changepoint_range	0.65	Selection of change points in the first 65% of the range.
	seasonality_prior_scale	0.50	The intensity of seasonality is 0.50.
Period II	Parameters	Set value	Interpretation
	growth	linear	Linear growth trend.
	seasonality	yearly	Annual seasonality.
	mcmc_samples	20,000	The MCMC sampling times are 20000.
	changepoint_prior_scale	0.29	The intensity of the growth trend is 0.29.
	changepoint_range	0.47	Selection of change points in the first 47% of the range.
	seasonality_prior_scale	0.50	The intensity of seasonality is 0.50.

[a] Note: "mcmc" means Monte Carlo Markov Chains. The mcmc_sample is to get the uncertainty of the predicted future. If greater than 0, full Bayesian inference will be done for MCMC samples, if it equals 0, maximum a posteriori estimation will be done, default setting is 0. Through trial-and-error experiments, with mcmc_sample = 2000, the model has a certain stability.

Table 10
Settings of holidays (events).

Period I		Period II	
2007–08	Outbreak of the subprime mortgage crisis.	2019–12	Starting point of the COVID-19 epidemic.
2008–09	Further escalation of the Global Financial Crisis.	2020–01	Epidemic lockdown policy in effect.
2008–10	Global stock market collapsed.	2021–02	Implementation of the mass vaccination program.
2009–01	The Economic Stimulus Bill was released.	2021–11	Epidemic restrictions eased, and social and economic activities resumed.
2009–06	The International Monetary Fund declared the global economy in deep recession.	2022–04	New variants caused a new COVID-19 wave of outbreaks, leading to closure and quarantine measures.
2010–07	The sovereign debt crisis erupted in Europe.		
2010–08	The sovereign debt crisis escalated In Europe.	2022–07	The World Health Organization and others emphasized the importance of continued compliance with anti-epidemic measures.
2011–01	The sovereign debt crisis worsened, spreading its effects to other European countries.		
2011–02	Countries around the world responded to the crisis with monetary policies and fiscal stimulus measures.	2022–10	Entry restrictions began to be eased, and international travel gradually resumed.
2012–01	Global economic situation began to show signs of easing.		

improved, and the MAE, MAPE, and RMSE are reduced by 11.81%, 11.38%, and 15.68%, respectively.

Considering the influence of Financial Crisis, clusters comprising the uncertainty indexes and numerous other indexes substantially enhance predictive effectiveness, as evidenced by decreased MAE, MAPE, and RMSE. The model that separately includes the AM-EMV, EPUS, and the P1_C2 variables shows superior forecasting performance compared to the model that focuses solely on the impact of the Financial Crisis, with a reduction in the MAE of 2.42%, 0.22%, and 2.25%, a reduction in the MAPE of 2.03%, 0%, and 2.03%, and a reduction in the RMSE of 0.80%, 0.48%, and −3.58%, respectively. The forecasting performance of the models incorporating AFR and EPUI, respectively, is lower only in terms of MAE compared to the Prophet model. Models incorporating EPUC, EPUJ, GEPU, and P1_C1 perform worse than the Prophet model.

Notably, P1_C2 is a clustered combination of EPUS and EPUC*. The model built upon this foundation performs better than the model that integrates the two uncertainty indexes individually. Therefore, simultaneously considering economic conditions of Spain and Chile would yield better results for forecasting BDI.

As shown in Table 12, to better understand the role of uncertainty indexes in forecasting BDI, we categorize the 10 uncertainty indexes in Period I into four gradients, and their forecasting effects on BDI are “significant”, “comparatively significant”, “common”, and “no effect”, respectively. The smaller the order of the gradients, the greater the positive effect of the uncertainty indexes in the corresponding level on the BDI forecast. The same applies to Period II.

Fig. 10, Fig. 11, and Fig. 12 illustrate the comparison of the variables' effects that significantly impact the forecasting of the BDI. The shaded area indicates the interval of significant effect of the uncertainty indexes, similarly hereinafter. Appendix A presents comparative plots of the effects of the models with the remaining variables added. The model incorporating the uncertainty indexes shows more robust performance from July 2010 to January 2011, primarily due to the lingering effects of the Financial Crisis and the European Debt Crisis.

From November 2001 to January 2012, the BDI experienced significant fluctuations due to the collapse of Lehman Brothers, the Global

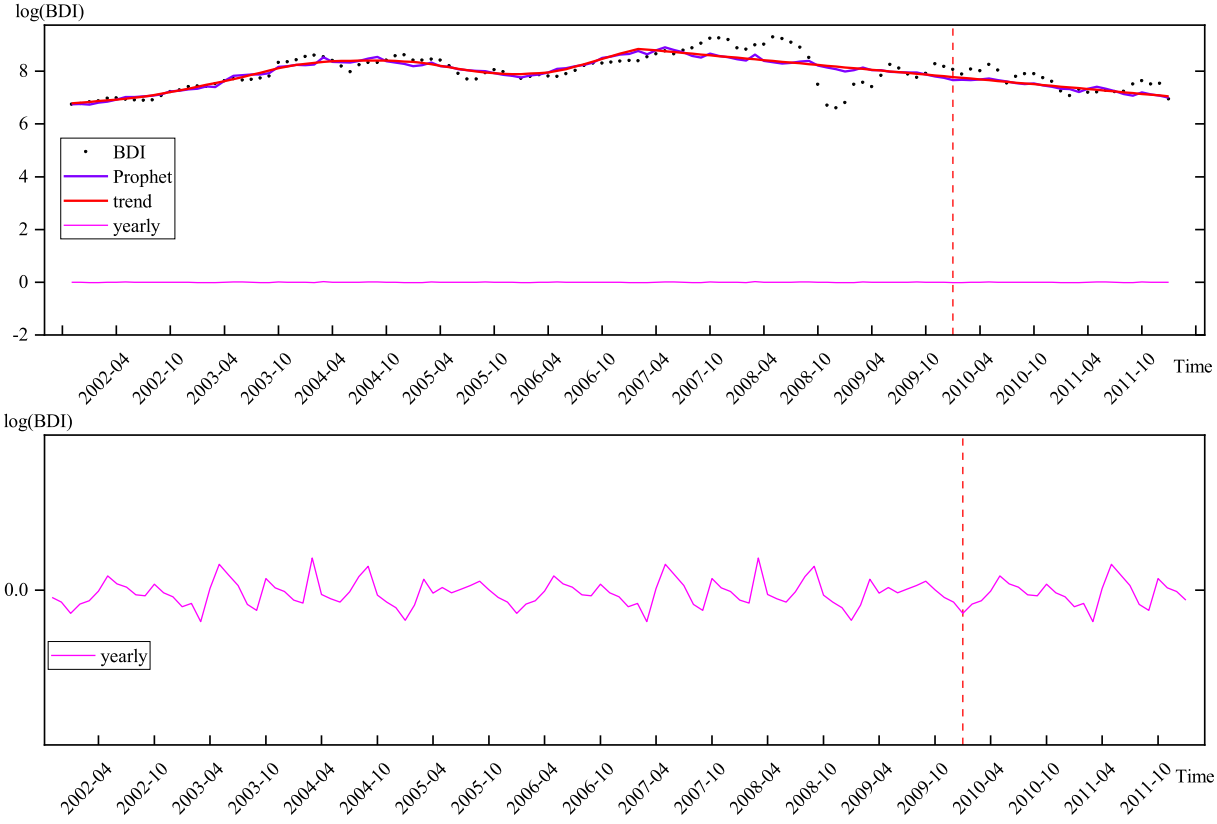

Fig. 8. Prophet model performance (Period I) (the lower sub-figure is a zoom-in view of “yearly” in the upper one, as is Period II).

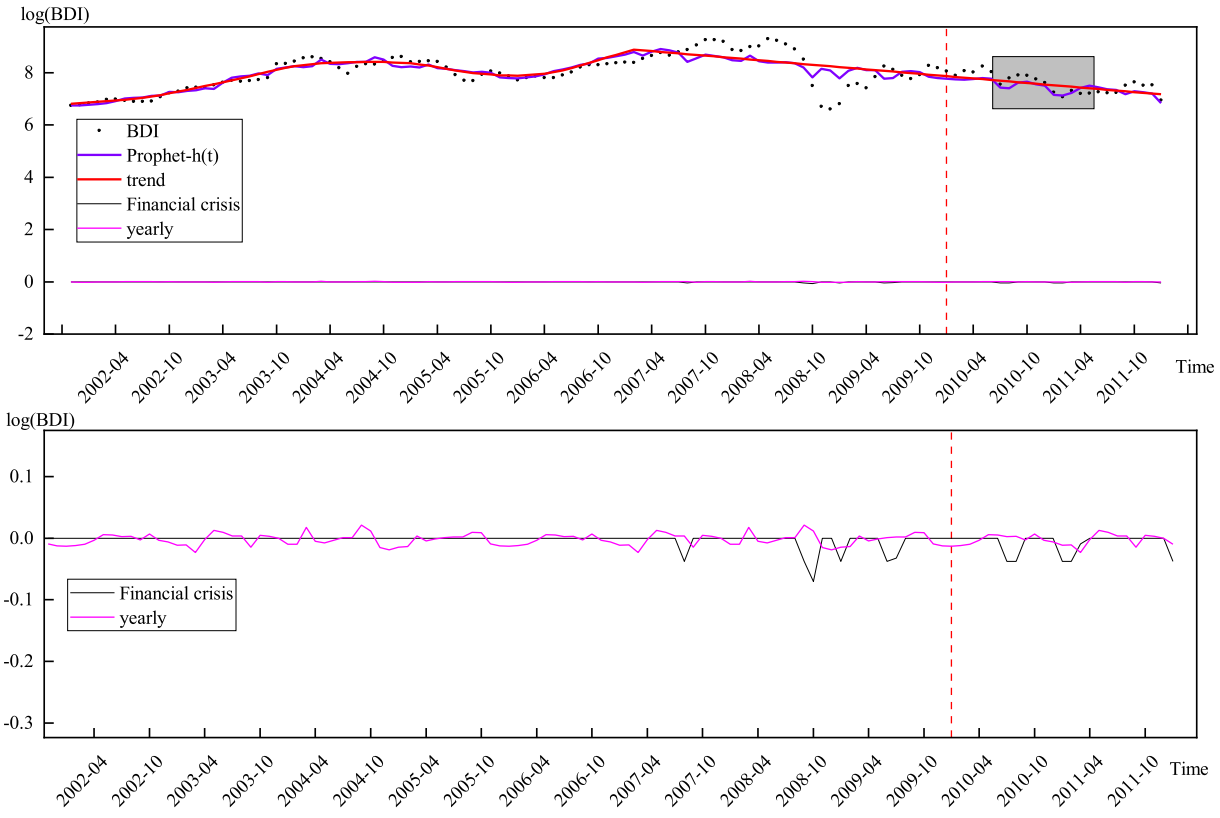

Fig. 9. Prophet model performance considering the impact of the Financial Crisis (Period I) (the lower sub-figure is a zoom-in view of "yearly" and "holidays" in the upper one, as is Period II).

Table 11
Prophet model forecasting considering Financial Crisis and uncertainty indexes (Period I).

Factors [a]	MAE	MAPE	RMSE	Outliers
-	0.2575	0.0334	0.2979	0
$h(t)$	0.2271	0.0296	0.2512	0
$h(t) + x_{10}$	0.2316	0.0304	0.2626	0
$h(t) + x_{11}$	0.4865	0.0648	0.6410	0
$h(t) + x_{12}$	0.2412	0.0315	0.2822	0
$h(t) + x_{13}$	0.3185	0.0426	0.3870	0
$h(t) + x_{14}$	0.2939	0.0394	0.3652	0
$h(t) + x_{15}$	0.2543	0.0341	0.3111	0
$h(t) + x_{16}$	0.2529	0.0340	0.3170	0
$h(t) + x_{17}$	**0.2216**	**0.0290**	**0.2492**	0
$h(t) + x_{18}$	0.2266	0.0296	0.2500	0
$h(t) + x_{19}$	0.2411	0.0319	0.3027	0
$h(t)$ +P1_C1 [b]	0.2922	0.0390	0.3415	0
$h(t)$ + P1_C2	0.2220	**0.0290**	0.2602	0
$h(t)$ + P1_C3	0.2322	0.0309	0.2712	0

[a] Note: "-" represents the baseline Prophet model; "$h(t)$" indicates that the impact of momentous events is taken into account based on the baseline Prophet model, and the "Prophet + $h(t)$" model is formed; "$h(t) + x_{ij}$" indicates that uncertainty indexes are taken into account based on the "Prophet+$h(t)$" model, and the "Prophet + $h(t) + x$" model is formed. The same as Tables 12 and 21.

[b] Note: in this paper, the variables in the clustered portfolio are averaged as the clustered portfolio values.

Table 12
Positive effect rating of 10 variables on BDI forecasting in Period I.

Levels	Variables	Effect rating	The performance of Prophet+$h(t)$+x
First gradient	x_{17}(AMEMV) x_{18}(EPUS) P1_C2	Significant	Performs better than Prophet+$h(t)$.
Second gradient	x_{10}(EPUK) x_{12}(EPUA) x_{19}(EPUC*) P1_C3	Comparatively significant	Performs a little worse than Prophet+$h(t)$, but better than Prophet.
Third gradient	x_{15}(AFR) x_{16}(EPUI)	Common	Performs almost the same as Prophet.
Fourth gradient	x_{11}(EPUC) x_{13}(EPUJ) x_{14}(GEPU) P1_C1	No effect	Performs even worse than Prophet.

Financial Crisis, and the European Debt Crisis, severely impacting global economies. Although leading indicators picked up as the economy recovered, recessionary conditions persisted for over two years (Notteboom, Pallis, & Rodrigue, 2021). The results lead to the following conclusions: the shipping industry was predominantly affected by the economies of Europe and the Americas during the Financial and European Debt Crises.

The Financial Crisis caused a decrease in demand for the dollar in different nations. The ensuing European Debt Crisis further challenged the stability of the eurozone as a whole and destabilized the role of the eurozone countries in the global monetary system. The crisis first punched eurozone countries such as Spain, the UK, and Ireland, as well as dollar zone countries such as America. Therefore, considering the economies of those countries will effectively improve the predictive ability of the BDI.

4.4.4. *Forecasting results for Period II*

The Prophet model was utilized to train and forecast the BDI for Period II. The results are illustrated in Fig. 13 and Fig. 14. The annual seasonal subseries obtained by decomposition changes when the impact of the COVID-19 epidemic is added to the model. The Prophet model, which considers the impact of the COVID-19 epidemic, shows enhanced ability in both in-sample and out-of-sample settings (as shown in the

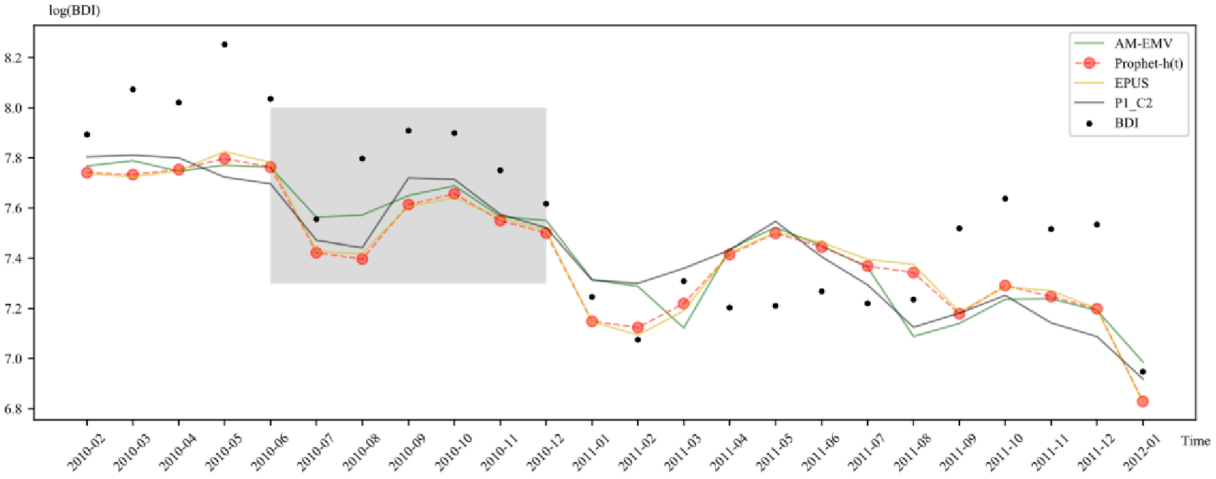

Fig. 10. Forecasting comparison of the first gradient variables (Period I).

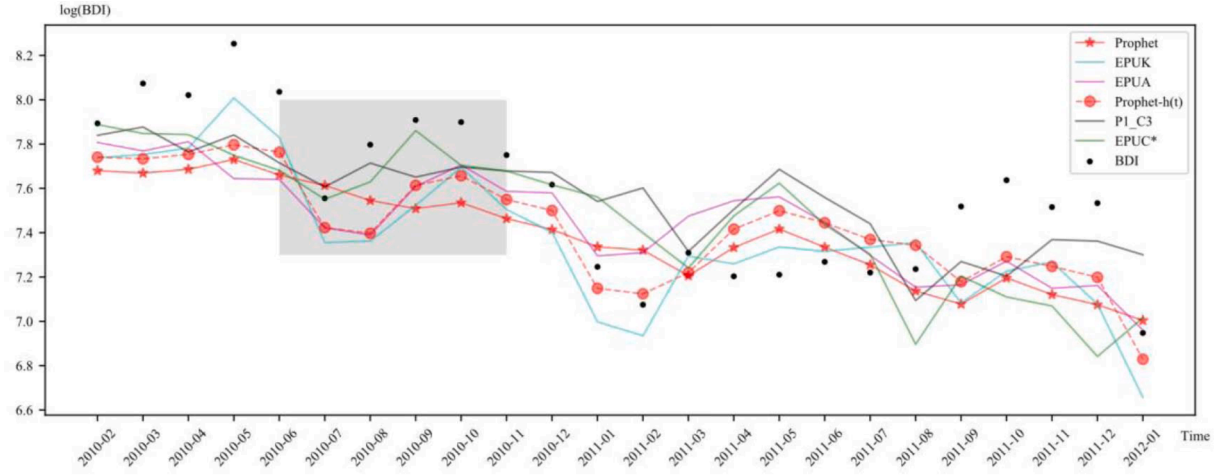

Fig. 11. Forecasting comparison of the second gradient variables (Period I).

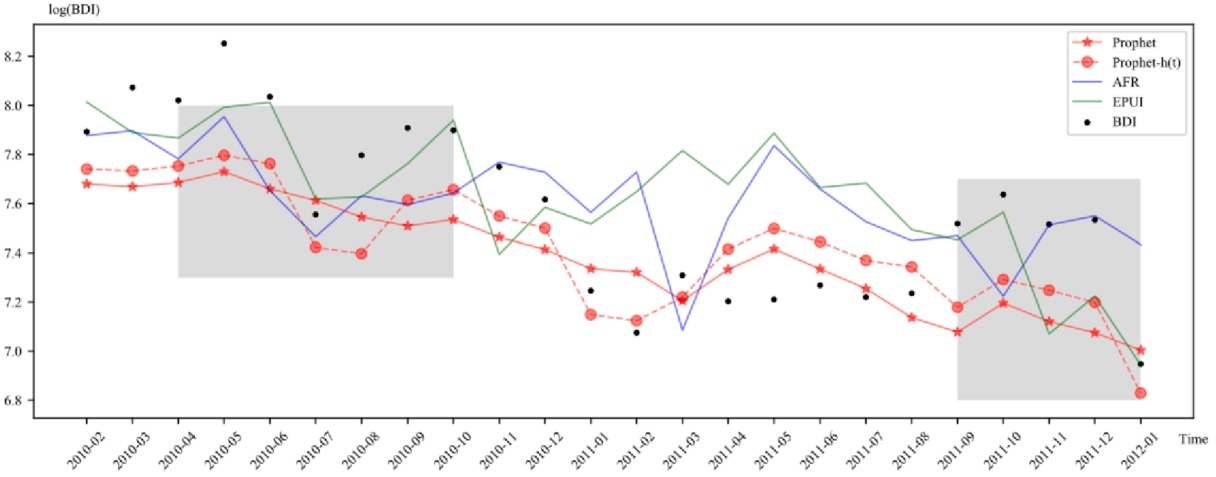

Fig. 12. Forecasting comparison of the third gradient variables (Period I).

shaded area) despite its lower effectiveness in forecasting the quickly expanding BDI during the period from November 2020 to October 2021. Similarly, in Period II, the 10 uncertainty indexes and their clustering combinations were added to the model separately, and the out-of-sample validation results are shown in Table 13. In Period II, the forecasting of the model considering the effect of the COVID-19 epidemic

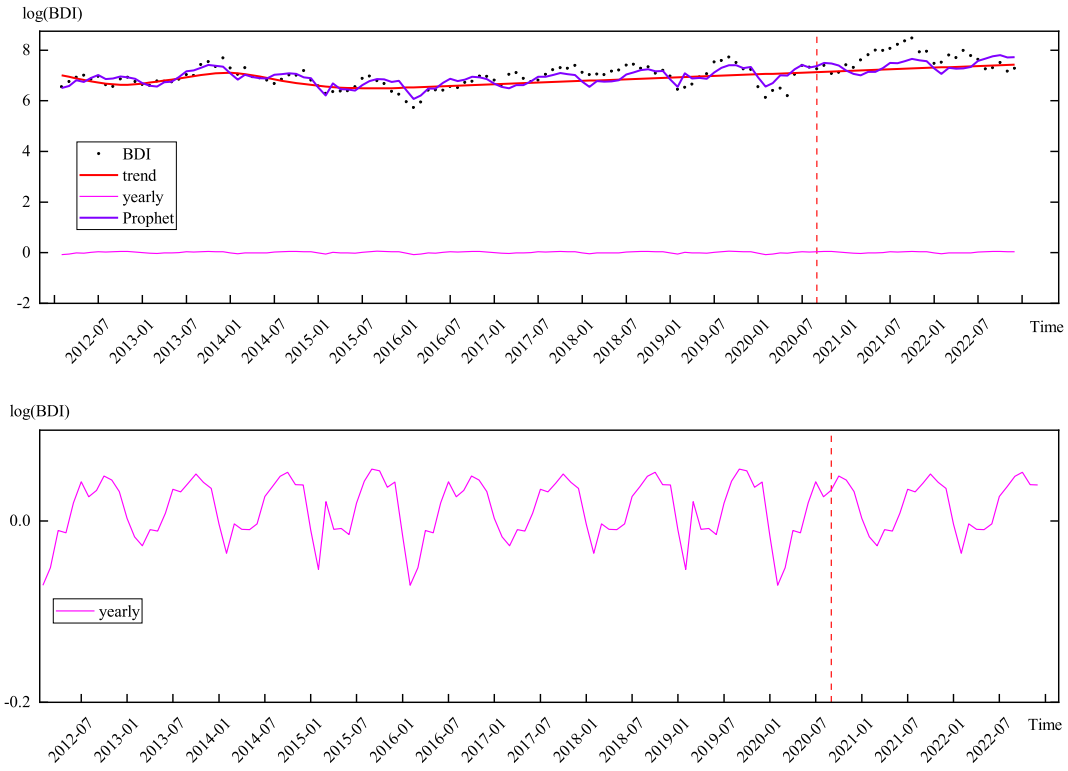

Fig. 13. Prophet model performance (Period II).

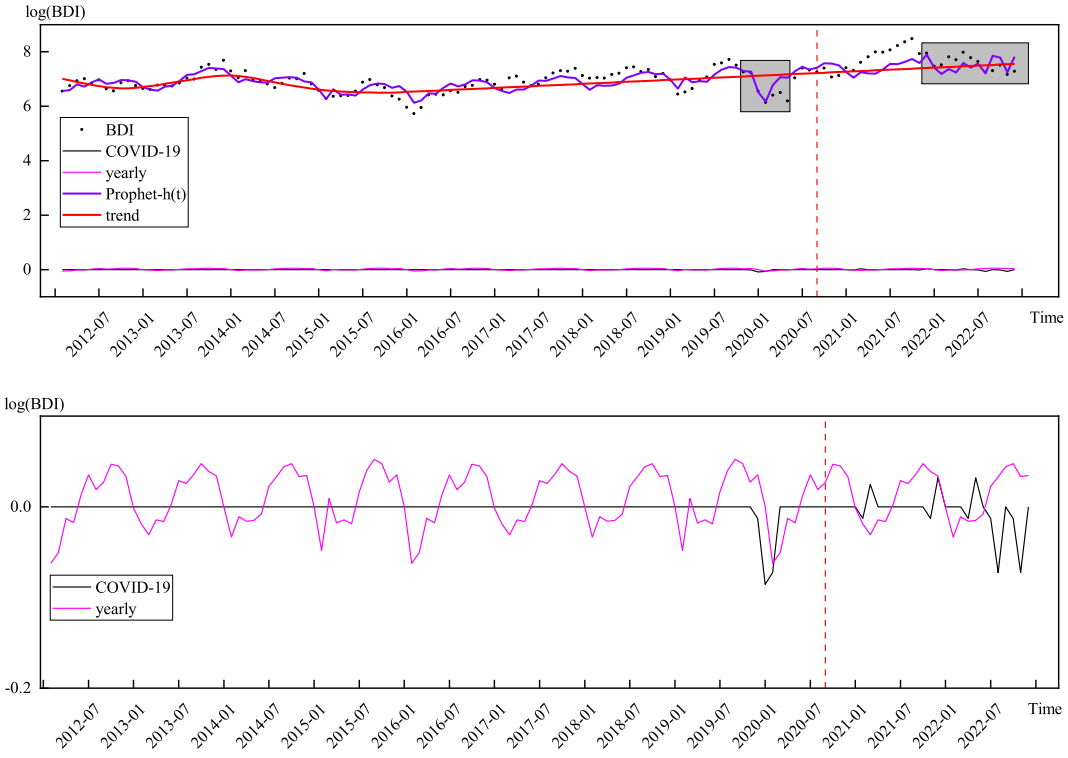

Fig. 14. Prophet model performance considering the impact of the COVID-19 (Period II).

was significantly improved, with the MAE, MAPE, and RMSE reduced by 16.95%, 17.05%, and 12.78%, respectively.

After sequentially incorporating uncertainty indexes into the model, combining other indexes and their clustering reduced model forecasting errors. However, this was not observed in the GPRT and P2_C3. Among them, the models with AI-EMV, GEPU, EPUS*, EPUAT, EPUC, P2_C1, and P2_C5, respectively, have higher forecasting accuracy than those that consider the impacts of the COVID-19 epidemic only, with a significant reduction in the number of anomalies.

Notably, P2_C1 is a clustered combination of EPUAT and AI-EMV.

Table 13
Prophet model forecasting considering the COVID-19 epidemic and uncertainty indexes (Period II).

Factors	MAE	MAPE	RMSE	Outliers
-	0.4689	0.0604	0.5150	1
$h(t)$	0.3894	0.0501	0.4492	1
$h(t) + x_{20}$	0.5594	0.0714	0.6444	5
$h(t) + x_{21}$	0.4369	0.0560	0.5108	0
$h(t) + x_{22}$	0.4359	0.0561	0.4876	1
$h(t) + x_{23}$	0.3858	0.0500	0.4477	1
$h(t) + x_{24}$	**0.2655**	**0.0351**	**0.3579**	**0**
$h(t) + x_{25}$	0.3047	0.0399	0.3961	0
$h(t) + x_{26}$	0.4213	0.0541	0.4795	1
$h(t) + x_{27}$	0.3809	0.0498	0.4609	0
$h(t) + x_{28}$	0.3873	0.0501	0.4578	0
$h(t) + x_{29}$	0.4060	0.0522	0.4629	1
$h(t)$ + P2_C1	0.3786	0.0494	0.4480	0
$h(t)$ + P2_C3	0.5055	0.0511	0.4556	4
$h(t)$ + P2_C5	0.3030	0.0399	0.3951	0

Table 14
Positive effect ratings of 10 variables on BDI forecasts in Period II.

Levels	Variables	Effect rating	The performance of Prophet+$h(t)$+x
First gradient	x_{23}(AI-EMV) x_{24}(GEPU) x_{25}(EPUS*) x_{27}(AEPUT) x_{28}(EPUC) P2_C1 P2_C5	Significant	Performs better than Prophet+$h(t)$.
Second gradient	x_{21}(EPUC**) x_{22}(EPUGT) x_{26}(WUI-TUR) x_{29}(CPU)	Comparatively significant	Performs a little worse than Prophet+$h(t)$, but better than Prophet.
Third gradient	x_{20}(GPR) P2_C3	No effect	Performs even worse than Prophet.

The forecasting of the model with the addition of P2_C1 is better than the model with the addition of the uncertainty index separately, which suggests that contagion affects the American stock market. The fiscal response measures taken by America will affect the volatility forecasting of the BDI. Thus, a combination of various American economic policies may positively affect the BDI forecasting.

The ranking of the 10 uncertainty indexes for forecasting the BDI in Period II is shown in Table 14. Fig. 15 and Fig. 16 show a comparison of the predictive effects of the models with the added variables. The onset of the COVID-19 epidemic in early 2020 resulted in a significant drop in the BDI. Later, there was a swift rise in the requirement for bulk carriers, leading to severe port congestion due to a surge in container freight rates. Countries adopted active economic policies to cope with the impact of the COVID-19 epidemic, and in October 2021, the BDI reached a new record high.

Based on the forecast results, four conclusions can be drawn:

(1) The economies of countries worldwide significantly impact the BDI during the COVID-19 epidemic, particularly those of Singapore and Canada, which are developed countries.
(2) The economic policies of China and America, as the trade war between these two countries intensifies, will also affect the fluctuation of the BDI significantly.
(3) The economic impact of climate change will permeate the global supply chain, international trade, and other channels. The extreme weather in Europe in 2021 resulted in a worldwide energy crisis. Suddenly, widening energy supply gaps triggered an increase in energy prices. The uncertainty of climate policy also reflects economic fluctuations to a certain extent, which can affect the BDI trend.
(4) Despite the wars and unstable world political situation in recent years, their impact on the BDI is relatively small in the short term.

4.5. Comparison experiment

4.5.1. Original benchmark models

On the one hand, to test the Prophet model's ability to decompose the time series features, it was compared to the ARIMA, SARIMA, and Three Order Exponential Smoothing (Holt-Winters) models. On the other hand, in order to experiment with the Prophet model's ability to learn autonomously, it was compared with the machine learning models (SVR and Relevance Vector Regression (RVR)) and deep learning models (ANN and LSTM). For the division of the training and test sets, benchmark models are consistent with Prophet. The baseline models are described as follows.

ARIMA: typically applies to single-column time-series data analysis, provided that the time-series data is smooth (or differentially processed if the data is not smooth);

SARIMA: abbreviated Seasonal ARIMA, that is, ARIMA with a seasonal component;

Holt-Winters: a method for forecasting non-stationary single-column series with linear trends and periodic fluctuations using cubic exponential smoothing and seasonal characteristics;

SVR: a regression method based on Support Vector Machine (SVM);

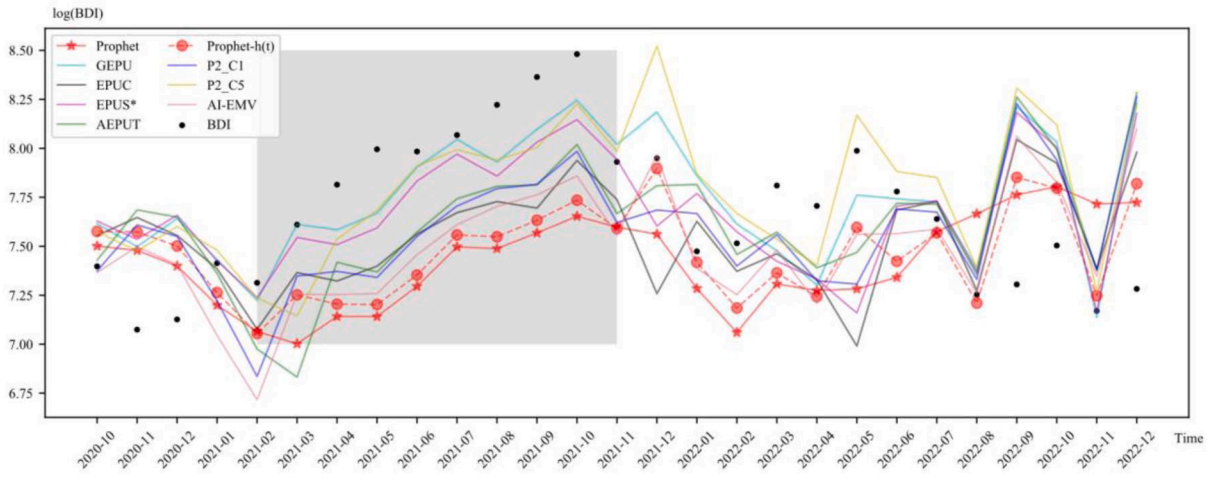

Fig. 15. Forecasting comparison of the first gradient variables (Period II).

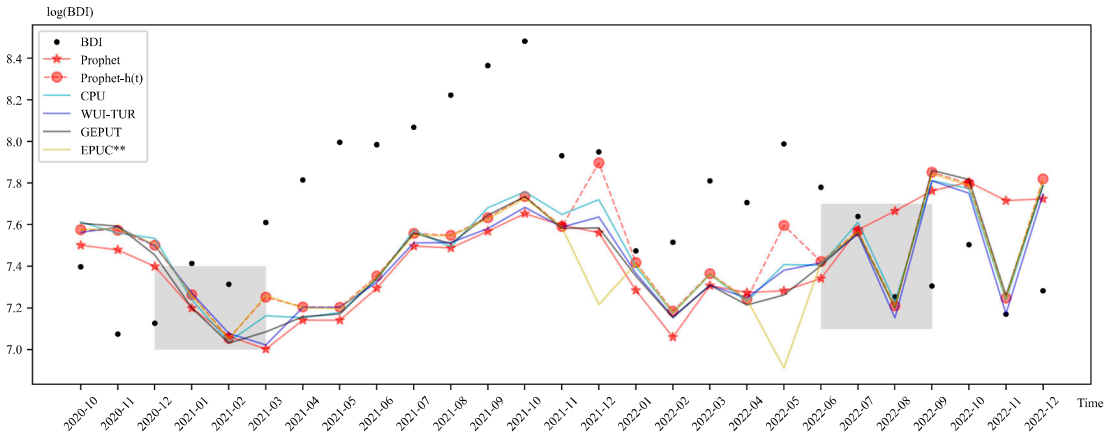

Fig. 16. Forecasting comparison of the second gradient variables (Period II).

Table 15
Models' settings.

Models	Key parameters	Parameterization methodology
ARIMA	"P", "d", "q"	Akaike information criterion (AIC)
SARIMA	"P", "d", "q", "P", "D", "Q"	Akaike information criterion (AIC)
Holt-Winters	"trend", "seasonal", "seasonal_periods"	Grid Search
SVR	"kernel", "C", "gamma"	Grid Search
RVR	"kernel", "Alpha", "gamma"	Grid Search
ANN	"epochs", "batch_size"	Grid Search
LSTM	"epochs", "batch_size"	Grid Search

RVR: a regression method based on Relevance Vector Machine (RVM);

ANN: a deep learning model based on the workings of biological neurons for specific tasks such as classification and prediction;

LSTM: a deep learning model for processing sequence data, which can solve the long-term dependency problem and is widely utilized in time series prediction and other fields.

All models are executed in Python and are implemented as Table 15. The out-of-sample performance of each model is shown in Table 16. Compared to other models, the Prophet+$h(t)$ model demonstrates superior forecasting capabilities. The basic Prophet significantly outperforms ARIMA, Holt-Winters, SVR, and RVR in Period I. However, it needs to demonstrate an enormous advantage over SARIMA, ANN, and LSTM. In Period II, the basic Prophet significantly outperforms ARIMA, SARIMA, SVR, and RVR but is worse than the Holt-Winters.

To visualize the forecasting performance of the models, Fig. 17 is attached. We did not put all the models into Fig. 17, and just selected models with the outstanding predictive performance in each period. Overall, we can draw the following three conclusions. (1) The Prophet model shows significant advantages over general time series models (ARIMA, SARIMA, and Holt-Winters) and machine learning models (SVR and RVR). Although the basic Prophet model did not perform significantly better than ANN and LSTM, the Prophet model has satisfactory interpretability, enables us to understand the intrinsic laws and external influences of the BDI, and has a simple structure, few parameters, and fast running speed. (2) The Prophet model, which considers the impact of momentous events, shows substantial predictive power for the BDI. (3) The BDI series is characterized by significant seasonality, and it is beneficial to consider seasonality in the model for forecasting, as both the SARIMA and Holt-Winters models take seasonality into account.

4.5.2. *Benchmark models with uncertainty indexes*

In addition, we add the uncertainty indexes as exogenous variables to some of the benchmark models to test the models' regression performance and the uncertainty indexes' actual role. Since SAIMA, ANN, and LSTM models perform sufficiently (Holt-Winters performs univariate forecasting), we compare the above three models considering uncertainty indexes with the Prophet model. We do not experiment with all 10 uncertainty indexes and select only the ones that perform competently in the BDI forecasts, i.e., the "first gradient" listed in Tables 12 and 14. The results are shown in Tables 17 and 18.

In Period I, the uncertainty indexes that play a significant role in BDI forecasting in the Prophet model also improve the forecast accuracy in SARIMA, ANN, and LSTM (except x_{17} in SARIMA). Moreover, Prophet still performs satisfactorily with the addition of the index. Same as Period I, in Period II, the uncertainty indexes that play a significant role in BDI forecasting in the Prophet model also improve the prediction accuracy in SARIMA, ANN, and LSTM. The Prophet model with the index added performs best most of the time.

Table 16
Comparison of model forecasting.

Period I				Period II			
Models	MAE	MAPE	RMSE	Models	MAE	MAPE	RMSE
Prophet	0.2575	0.0334	0.2979	Prophet	0.4688	0.0604	0.5150
Prophet+$h(t)$	**0.2271**	**0.0296**	**0.2512**	Prophet+$h(t)$	**0.3894**	**0.0501**	**0.4492**
$ARIMA_{(0,1,1)}$	0.5264	0.0717	0.6212	$ARIMA_{(2,0,0)}$	0.7588	0.0966	0.8620
$SARIMA_{(0,1,1)(0,1,1)}$	0.2763	0.0372	0.3520	$SARIMA_{(0,1,0)(1,1,0)}$	0.4873	0.0623	0.5749
Holt-Winters	0.4385	0.0593	0.5118	Holt-Winters	0.4434	0.0563	0.5308
SVR	0.6886	0.0907	0.7730	SVR	0.6260	0.0797	0.7341
RVR	0.5182	0.0695	0.5791	RVR	0.5851	0.0744	0.6929
ANN	0.2614	0.0344	0.2968	ANN	0.4687	0.0605	0.5224
LSTM	0.2619	0.0354	0.3181	LSTM	0.4707	0.0596	0.5497

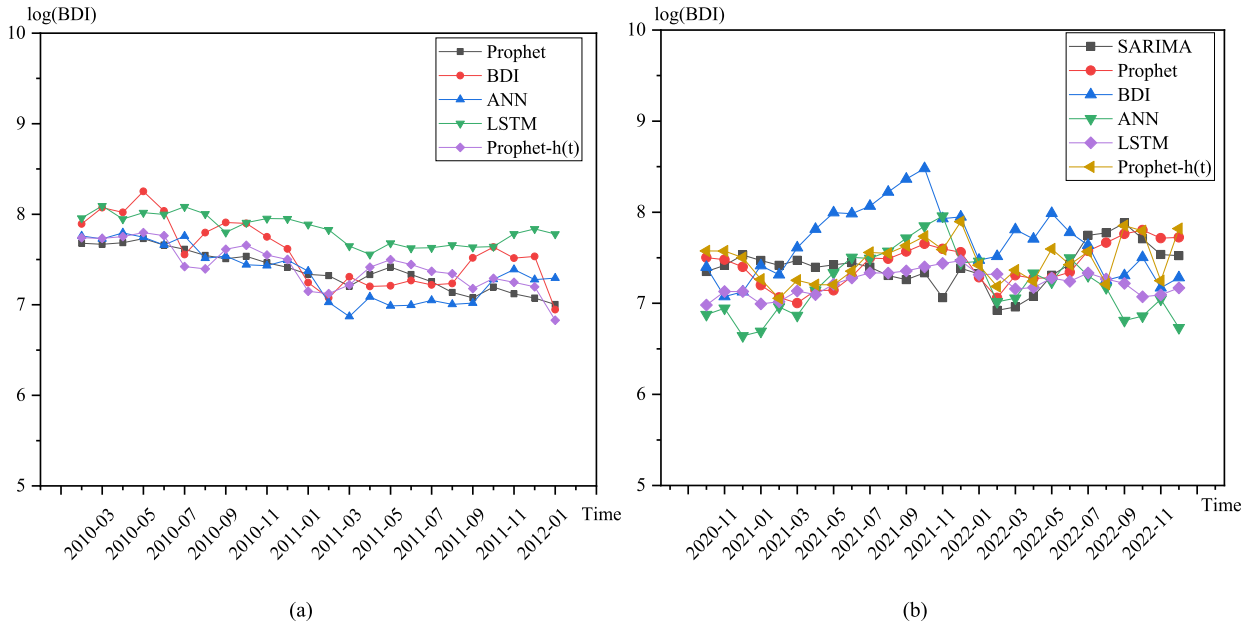

Fig. 17. (a) Comparison of models in Period I; (b) Comparison of models in Period II.

Table 17
Comparison of models considering uncertainty indexes (Period I).

Variables	Models	MAE	MAPE	RMSE	Variables	Models	MAE	MAPE	RMSE
-	Prophet	**0.2271**	**0.0296**	**0.2512**	x_{18}	Prophet	**0.2266**	**0.0296**	**0.2500**
	ANN	0.2616	0.0344	0.2968		ANN	0.2487	0.0366	0.3071
	LSTM	0.2619	0.0354	0.3181		LSTM	0.2461	0.0332	0.3052
	SARIMA	0.2763	0.0372	0.3520		SARIMA	0.2685	0.0362	0.3449
x_{17}	Prophet	**0.2216**	**0.0290**	**0.2492**	P1_C2	Prophet	**0.2220**	**0.0290**	**0.2602**
	ANN	0.2404	0.0325	0.3014		ANN	0.2451	0.0330	0.3691
	LSTM	0.2301	0.0310	0.2917		LSTM	0.2337	0.0314	0.2694
	SARIMA	0.2872	0.0385	0.3865		SARIMA	0.2688	0.0362	0.3453

Table 18
Comparison of models considering uncertainty indexes (Period II).

Variables	Models	MAE	MAPE	RMSE	Variables	Models	MAE	MAPE	RMSE
-	Prophet	**0.3894**	**0.0501**	**0.4492**	-	LSTM	0.4707	0.0596	0.5497
	ANN	0.4564	0.0589	0.5104		SARIMA	0.4873	0.0623	0.5749
x_{23}	Prophet	**0.3858**	**0.0500**	**0.4477**	x_{27}	Prophet	0.3809	0.0498	0.4609
	ANN	0.4137	0.0523	0.5663		ANN	**0.3566**	**0.0457**	0.4861
	LSTM	0.4246	0.0536	0.5166		LSTM	0.4038	0.0511	0.4849
	SARIMA	0.4804	0.0615	0.5587		SARIMA	0.4195	0.0542	**0.4595**
x_{24}	Prophet	**0.2655**	**0.0351**	**0.3579**	x_{28}	Prophet	0.3873	0.0501	0.4578
	ANN	0.3146	0.0406	0.4152		ANN	0.3969	0.0508	0.5461
	LSTM	0.3784	0.0478	0.4621		LSTM	0.3940	0.0498	0.4732
	SARIMA	0.4081	0.0527	0.4497		SARIMA	**0.3758**	**0.0488**	**0.4192**
x_{25}	Prophet	0.3047	0.0399	0.3961	P2_C1	Prophet	**0.3786**	0.0494	**0.4480**
	ANN	**0.2992**	**0.0388**	**0.3741**		ANN	0.4118	0.0531	0.5219
	LSTM	0.3845	0.0486	0.4687		LSTM	0.3794	**0.0479**	0.4646
	SARIMA	0.4216	0.0543	0.4659		SARIMA	0.4363	0.0562	0.4816
P2_C5	Prophet	**0.3030**	**0.0399**	**0.3951**	P2_C5	LSTM	0.3518	0.0444	0.4284
	ANN	0.3623	0.0471	0.4279		SARIMA	0.3792	0.0492	0.4199

5. Robustness tests

5.1. Adjustment of sample period

5.1.1. Period consolidation

We test the validity of the models employed in this paper through this section. We process the sample set as a whole, i.e., without dividing it into Period I and Period II, and the steps performed are the same as in Section 4. After the merging, some uncertainty indexes contain many consecutive missing values. The paper did not utilize interpolation but directly executed those indexes, so 355 uncertainty indexes were initially screened for the whole period.

(1) MIC-Boruta.

The 355 uncertainty indexes mentioned above were screened using the MIC-Boruta algorithm, i.e., 10 variables were screened for higher correlation with the BDI. However, considering the economic significance among the variables, we adjusted the screened 10 indexes. Specifically, the correlation between the Greek Economic Policy

Table 19
Definition of the relevant variables (whole period).

Just statistical (before adjustment)		Statistical and economic (after adjustment)	
Definition (abbreviation)	Correlation	Definition (abbreviation)	Correlation
Canadian Economic Policy Uncertainty (EPUC)	0.46	Canadian Economic Policy Uncertainty (EPUC)	0.46
Japan trade policy uncertainty (TPUJ)	0.46	Japan trade policy uncertainty (TPUJ)	0.46
Global Economic Policy Uncertainty (GEPU)	0.40	Global Economic Policy Uncertainty (GEPU)	0.40
Greek Economic Policy Uncertainty (EPUG)	0.38	European Economic Policy Uncertainty (EPUE)	0.38
European Economic Policy Uncertainty (EPUE)	0.38	UK Economic Policy Uncertainty (EPUK)	0.38
UK Economic Policy Uncertainty (EPUK)	0.38	China Economic Policy Uncertainty (EPUC*)	0.37
China Economic Policy Uncertainty (EPUC*)	0.37	America Financial Crises EMV Tracker (AFCEMV)	0.36
America Financial Crises EMV Tracker (AFCEMV)	0.36	Swiss Economic Policy Uncertainty (EPUSW)	0.35
Swiss Economic Policy Uncertainty (EPUSW)	0.35	Turkey Geopolitical Risk Index (TGR)	0.35
Turkey Geopolitical Risk Index (TGR)	0.35	Italia Economic Policy Uncertainty (EPUIT)	0.35

Uncertainty Index and the BDI is 0.38, and the Turkish Geopolitical Risk Index is 0.35, as is Italian Economic Policy Uncertainty Index. Italy and Greece are both European countries, but considering their economic and shipping status, we replace the Greek economic policy uncertainty index with the Italian economic policy uncertainty index. The results are shown in Table 19. There is a difference in the screened uncertainty indexes after the merging phase compared to Period I and Period II.

(1) K-Shape.

The above 10 indexes were clustered using the K-Shape algorithm and co-clustered into 4 categories, as shown in Fig. 18.

(2) Prophet forecasting.

In order to make the momentous event (COVID-19) influence the training part to the test part and make the test set contain a different sample than Period II, the training part was set to 2001–11 to 2020–05, and the test part was set to 2020–06 to 2022–12, roughly a 90%-10% ratio.

Standing at the point in time of May-June 2020, which is six months after the start of the COVID-19 epidemic, the situation seems to be improved, but we do not know what direction the future will take, so when modeling the impact of the epidemic, we set it up based on the training set. This is different from the setup for "holiday" in Period II. The settings of "holiday" are shown in Table 20, and the out-of-sample validation results are shown in Table 21.

The forecasting results show that, when the impact of COVID-19 is considered, the performance of the Prophet is significantly improved, with its MAE, MAPE, and RMSE decreasing by 23.44%, 21.06%, and 23.69%, respectively. Furthermore, the forecasting performance continues to improve after adding certain uncertainty indexes. Specifically, EPUE plays the most critical role in forecasting BDI, followed by GEPU, EPUIT, and EPUSW.

Interestingly, the forecasting improved when Cluster 1 (a

Table 20
Setting of "holiday" (whole period).

Time	lower_window [a]	upper_window
2019–12	0	36
2020–01	0	36
2020–02	0	36
2020–03	0	36
2020–04	0	36
2020–05	0	36

[a] Note: lower_window and upper_window are the impact interval of the holiday. Setting it to 36 assuming that the COVID-19 can affect the following three years.

Table 21
Prophet model forecasting considering the COVID-19 epidemic and uncertainty indexes (whole period).

Factors	MAE	MAPE	RMSE	Outliers
-	0.4138	0.0527	0.5079	6
$h(t)$	0.3168	0.0416	0.3876	0
$h(t)$ + EPUC	0.3674	0.0493	0.4873	2
$h(t)$ + TPUJ	0.3494	0.0467	0.4347	0
$h(t)$ + GEPU	**0.2819**	0.0377	0.3680	0
$h(t)$ + EPUE	0.2823	**0.0371**	**0.3341**	**0**
$h(t)$ + EPUK	0.3186	0.0424	0.3922	0
$h(t)$ + EPUC *	0.3259	0.0438	0.4193	0
$h(t)$ + AFCEMV	0.3171	0.0419	0.3854	0
$h(t)$ + EPUSW	0.3097	0.0406	0.3742	1
$h(t)$ + TGR	0.3170	0.0416	0.3824	0
$h(t)$ + EPUIT	0.3014	0.0397	0.3719	0
$h(t)$ + Cluster1	0.3142	0.0415	0.3777	0
$h(t)$ + Cluster 2	0.4020	0.0541	0.5441	1

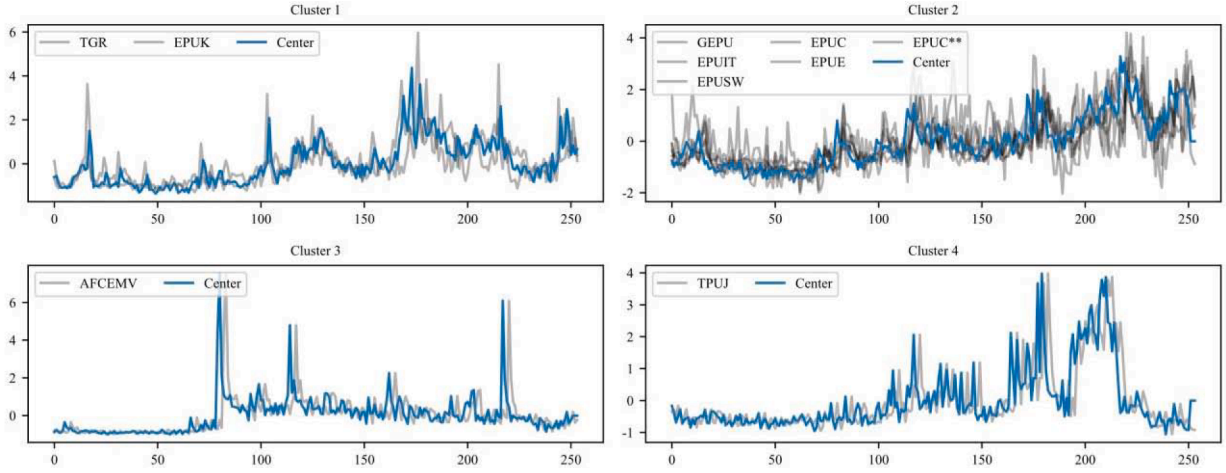

Fig. 18. K-Shape clustering results (whole period).

Table 22
Positive effect ratings of 10 variables on BDI forecasts (whole period).

Levels	Variables	Intercontinental	Effect rating	The performance of Prophet+$h(t)$+x
First gradient	GEPU	Globe	Significant	Performs better than Prophet+$h(t)$.
	EPUE	Europe		
	EPUSW			
	EPUIT			
Second gradient	AFCEMV	North America	Comparatively significant	Performs a little worse than Prophet+$h(t)$, but better than Prophet.
	EPUC			
	EPUC*	Asia		
	TPUJ			
	TGR			
	EPUK	Europe		

combination of TGR and EPUK) was added to the model. This suggests that considering both TGR and EPUK can improve the prediction accuracy of BDI. This is precisely the point of using K-Shape clustering in this paper, i.e., to tap into the combined effects between different variables that are seemingly unrelated.

The indexes are categorized into two gradients based on their predicted performance, as shown in Table 22. The 10 significant uncertainty indexes are mainly from European, North American, and Asian countries. The indexes that contribute significantly to the BDI forecast, except for GEPU, are affiliated with European countries.

Asia, Europe, and North America occupy a considerable share of the world's trade from the existing trade pattern. At the same time, maritime transport takes up about 90% of the transportation in international trade. The shipping geography of Europe is critical. The large number of its countries leads to the need to route through several countries after arriving at the port from some ocean containers, involving a large amount of transit transport. Hence, the complexity of containerized trade in Europe exceeds that of Asia and North America to a certain extent.

Finally, we add EPUG (which has been replaced by EPUIT) into the model, and the results of MAE, MAPE, and RMSE are 0.3639, 0.0487, and 0.4225, respectively, which are significantly worse than that of EPUIT. This shows that in actual forecasts, we cannot rely only on mathematical methods but also combine the actual interpreted meanings of the variables to grasp the link between input and output variables.

Overall, the models employed remain stable in their performance when we examine the entire sample set. This is demonstrated by the fact that, firstly, the MIC-Boruta feature screening method is able to reduce the dimensionality of the input variables and filter out the indexes that have a more significant effect on the forecasting of the BDI from some indexes. Secondly, adding the clustered combinations obtained through the K-Shape clustering method to the model can produce more acceptable results than a single variable in the combination, which suggests that K-Shape can tap the potential connection between variables to a certain extent, which is easily overlooked. Finally, the Prophet model provides us with a powerful tool for modeling the impact of momentous events, which can still significantly improve the accuracy of BDI forecasts when only the time point of the event and its future impact interval are set in the training set.

Table 23
Statistical description of the sample for the robustness test.

Periods	Proportion of division	Phases
Period I	70%-30%	2001–11 to 2009–01
		2009–02 to 2012–01
	90%-10%	2001–11 to 2011–01
		2011–02 to 2012–01
Period II	70%-30%	2012–02 to 2019–08
		2019–09 to 2022–12
	90%-10%	2012–02 to 2021–10
		2021–11 to 2022–12

5.1.2. Changing the ratio of training and test parts

The predictive capacity of the Prophet model in BDI forecasting is confirmed by changing the size of training and test samples. The proportion of training and test samples in Periods I and II is changed to 70%-30% and 90%-10% according to the "holiday" module setting principle of the Prophet model. The validation results are shown in Table 23. The Prophet model results are shown in Table 24.

The results of the comparison tests are shown in Table 25 and Table 26. As can be seen from Table 25, whether in Period I or Period II, the Prophet model outperforms all other models when adjusting the ratio of the training and test sets by 70%-30%. As shown in Table 26, the Prophet model performs competently when adjusting the training and test sets ratio to 90%-10% in Period I. In contrast, the LSTM and ANN models outperform the Prophet model in Period II. This may be because neural networks tend to overfit smaller data sets. In other words, it ends up remembering trained data and is often unable to generalize with new features in the test model.

We utilize the standard deviation of the errors to measure the stability of the model based on 3 ratios when the ratio of the training sample to the test sample changes. See Table 27. It can be seen that in Period I, the deep learning models (ANN and LSTM) have the best stability, followed by the Prophet model; in Period II, the Prophet model has the best stability.

In summary, combining the results of both sample divisions, the Prophet exhibits stronger robustness. In Period I, the Prophet model plays steadily and still outperforms the other 7 compared models. In Period II, the Prophet significantly outperforms ARIMA, SARIMA, SVR and RVR, and slightly outperforms Holt-Winters, ANN, and LSTM.

5.2. Sample size expansion

Based on the Period II study, the test sample set has been extended until August 2023. The data from February 2012 to September 2020 comprises the training samples, while the data from October 2020 to August 2023 comprises the test samples. Meanwhile, this section provides additional insights into the impact of the COVID-19 epidemic through the module in the Prophet model. The critical time nodes of the Russia-Ukraine conflict are set to realize the complementary study of momentous events. The essential time nodes of the COVID-19 epidemic and the Russia-Ukraine conflict are shown in Table 28. The Prophet model predictions are shown in Table 29.

In February 2022, the conflict between Russia and Ukraine erupted, leading to significant instability in the global financial markets. Risk aversion in the market has increased due to the rising risk of assets, including short equities and emerging market currencies, and the surge in trading prices for bulk commodities like energy and agricultural products. Based on Russia and Ukraine's vital position in the

Table 24
Prophet model results.

Periods	Sample Segmentation	Models	In-sample			Out-of-sample		
			MAE	MAPE	RMSE	MAE	MAPE	RMSE
Period I	70%-30%	Prophet	0.2789	0.0348	0.4007	0.3100	**0.0400**	**0.3720**
		Prophet+$h(t)$	**0.2576**	**0.0323**	**0.3822**	**0.3094**	0.0408	0.3992
	90%-10%	Prophet	0.2562	0.0323	0.3764	0.2363	0.0324	0.2588
		Prophet+$h(t)$	**0.2523**	**0.0318**	**0.3633**	**0.2258**	**0.0310**	**0.2552**
Period II	70%-30%	Prophet	**0.1684**	**0.0248**	**0.1575**	**0.4156**	**0.0583**	**0.4913**
		Prophet+$h(t)$[a]	**0.1684**	**0.0248**	**0.1575**	**0.4156**	**0.0583**	**0.4913**
	90%-10%	Prophet	0.2011	0.0288	0.1697	0.4455	0.0605	**0.4913**
		Prophet+$h(t)$	**0.1879**	**0.0269**	**0.1640**	**0.3396**	**0.0458**	0.4960

[a] Note: according to the setting principle of "holiday", when the ratio of training samples to test samples in Period II was changed to 70%-30%, the impact of the COVID-19 epidemic does not play a role in the Prophet + $h(t)$ model. Thus, the results are the same as the Prophet model.

Table 25
Comparison of model forecasting (70%-30%).

Period I				Period II			
Models	MAE	MAPE	RMSE	Models	MAE	MAPE	RMSE
Prophet	**0.3100**	**0.0400**	**0.3720**	Prophet	**0.4156**	0.0583	**0.4913**
$ARIMA_{(0,1,2)}$	0.7366	0.0939	0.8214	$ARIMA_{(2,0,0)}$	0.6583	0.0869	0.7653
$SARIMA_{(0,1,1)(0,1,1)}$	0.4660	0.0612	0.5505	$SARIMA_{(0,1,0)(3,1,0)}$	0.4495	0.0635	0.5776
Holt-Winters	0.5329	0.0654	0.6795	Holt-Winters	1.3712	0.2030	1.4609
SVR	0.4846	0.0649	0.5800	SVR	0.6257	0.0826	0.7215
RVR	0.5008	0.0663	0.5618	RVR	0.6093	0.0844	0.6698
ANN	0.3622	0.0477	0.4202	ANN	0.4310	**0.0575**	0.4987
LSTM	0.3162	0.0423	0.3924	LSTM	0.4404	0.0579	0.5170

Table 26
Comparison of model forecasting (90%-10%).

Period I				Period II			
Models	MAE	MAPE	RMSE	Models	MAE	MAPE	RMSE
Prophet	**0.2363**	**0.0324**	**0.2588**	Prophet	0.4455	0.0605	0.4960
$ARIMA_{(0,1,1)}$	0.2617	0.0353	0.3124	$ARIMA_{(2,0,0)}$	0.8878	0.1183	0.9270
$SARIMA_{(0,1,1)(0,1,1)}$	0.2812	0.0380	0.3430	$SARIMA_{(0,1,0)(0,1,2)}$	0.6301	0.0847	0.7516
Holt-Winters	0.5192	0.0645	0.6151	Holt-Winters	1.1171	0.1656	1.2707
SVR	0.5706	0.0786	0.6198	SVR	0.5768	0.0747	0.6944
RVR	0.6005	0.0788	0.7135	RVR	0.6156	0.0802	0.7213
ANN	0.2669	0.0364	0.2917	ANN	0.3809	0.0509	0.4522
LSTM	0.2677	0.0366	0.2910	LSTM	**0.3777**	**0.0488**	**0.4408**

international oil, natural gas, and grain markets, the Russian-Ukrainian conflict has a disruptive effect on the international shipping market, which has a more influential impact on the global industrial chain and supply chain. Based on the empirical results in this section, it is clear that the Prophet model has strong BDI predictive capabilities even when the sample period is extended. The model's adaptability to new momentous emergencies and conflicts is significantly more reasonable.

Table 27
The stability of each model.

Models	Period I			Period II		
	MAE	MAPE	RMSE	MAE	MAPE	RMSE
Prophet	0.0310	0.0034	0.0469	0.0218	**0.0010**	**0.0102**
ARIMA	0.1943	0.0242	0.2094	0.0939	0.0131	0.0664
SARIMA	0.0883	0.0111	0.0958	0.0778	0.0103	0.0827
Holt-Winters	0.0416	**0.0027**	0.0691	0.3915	0.0622	0.4012
SVR	0.0836	0.0105	0.0832	0.0231	0.0033	0.0166
RVR	0.0435	0.0053	0.0678	**0.0131**	0.0041	0.0211
ANN	0.0463	0.0059	**0.0124**	0.0360	0.0040	0.0292
LSTM	**0.0243**	0.0030	0.0429	0.0387	0.0047	0.0456

6. Conclusions and outlook

6.1. Conclusions

Accurate forecasting of the BDI is an excellent guide to understanding the changing law of freight rates and the dry bulk shipping market situation. It aids in measuring the prosperity of global trade and predicting the trend of the world economy. In addition, it offers crucial decision-making reference for shipping market participants to mitigate risks and seize opportunities.

Given the cyclical nature of the BDI and its susceptibility to the impact of the external environment, this paper proposes a BDI forecasting model based on the Prophet, taking into account the impact of multi-dimensional significant events, and draws the following main conclusions:

(1) The impact of non-cyclical emergencies on the shipping market is significant. The accuracy of BDI forecasting is significantly improved after incorporating the impact of the Financial Crisis and COVID-19 epidemic into the model.
(2) Various policies adopted by countries to cope with the impact of external emergencies, particularly economic policies, will cause

Table 28
Setting of holidays (events) (expansion period).

COVID-19 epidemic		Russia-Ukraine conflict	
2019–12	Starting point.	2022–02	Starting point.
2020–01	Epidemic lockdown policy in effect.	2022–06	Ukraine receives the Status of EU candidate country.
2021–02	Implementation of the mass vaccination program.	2022–07	The "Black Sea Agreement" was signed.
2021–11	Epidemic restrictions eased, and social and economic activities resumed.	2022–09	The "Nord Stream" gas pipeline was blown up.
2022–04	New variants caused a new wave of COVID-19 outbreaks, leading to closure and quarantine measures.	2023–01	The Russian-Ukrainian conflict widened in scale.
2022–07	The World Health Organization and others emphasized the importance of continued compliance with anti-epidemic measures.		
2022–10	Entry restrictions began to be eased, and international travel gradually resumed.	2023–02	Sanctions against Russia continue to escalate.
2023–05	Second wave of COVID-19 outbreaks.		

Table 29
Prophet model predictions (expansion period).

Models	In-sample			Out-of-sample		
	MAE	MAPE	RMSE	MAE	MAPE	RMSE
Prophet	0.2123	0.0312	0.1766	0.4657	0.0616	0.2482
Prophet + COVID-19	**0.1977**	**0.0290**	**0.1704**	0.4324	0.0575	0.2398
Prophet + COVID-19 + Russia-Ukraine conflict	**0.1977**	**0.0290**	**0.1704**	**0.4273**	**0.0566**	**0.2378**

fluctuations in the BDI. During the Financial Crisis, European countries (Spain and the UK) and the Americas (America and Chile) were the first to be affected by the Financial Crisis and the European Debt Crisis. Therefore, including financial market fluctuations and economic policy uncertainty in the European and American models can improve the BDI predictive ability. When analyzing the impact of the COVID-19 pandemic, implementing embargoes has resulted in international trade restrictions due to the virus spreading worldwide rapidly. The uncertainty of global economic policy has the most significant impact on BDI. Developed economies such as Singapore, America, and Canada also significantly affect BDI. In addition, climate change and global uncertainty have some impact, but they are insignificant.

(3) In practical forecasting, we can utilize the mathematical approach to capture the genuine relationship between the variables and the economic interpretation to grasp the actual relationship between the variables fully. As the results show, not all indexes screened for higher correlation with the BDI based on mathematical and theoretical methods alone will yield excellent results for BDI forecasting. Conversely, potential variables can be missed if statistical methods do not consider empirical experience alone.
(4) The Prophet model has a more satisfactory forecasting performance. Comparing and analyzing the performance of three time series models, ARIMA, SARIMA, and Holt-Winters, two machine learning models, SVR and RVR, and two deep learning models, ANN and LSTM, in forecasting the BDI, the results confirm that the Prophet model has higher accuracy, robustness, and stability in forecasting the BDI.

6.2. Future prospects

The emergence of significant international natural disasters and manufactured events, such as the SARS epidemic, the Financial Crisis, the Islamic State terrorist bloodshed, and the COVID-19 epidemic sweeping the globe, is highly likely to affect the global political and economic order. The results of this paper demonstrate that incorporating two momentous emergencies, the Financial Crisis and the COVID-19 epidemic, into the model dramatically enhances the forecasting accuracy of the BDI and enables the model to fit crucial mutation points effectively. Therefore, establishing a shared information platform to monitor uncertain events and creating an intelligent early warning system for crisis events in the shipping market is urged. Sharing data and filling up the broken points in the data chain of the shipping market will have a far-reaching positive impact on the industry, supply, and logistics chains.

Certain areas of this study deserve further elaboration:

(1) This paper utilizes the MIC-Boruta method to select only the top 10 uncertainty indexes with a higher correlation to BDI, which somewhat ignores the economic implications between the variables. The potential impact of additional uncertainty indexes can be explored in future research. In the future, applying more accurate feature selection algorithms or cross-validation strategies will give it more practical significance, not just statistical.
(2) Three parameters were estimated in this paper using the Grid Search method for the Prophet model in minimum increments of 0.01 steps. More precise and effective parameter estimation can be conducted for multiple parameters in the future.
(3) Looking at the volatility of the BDI, it would have been more appropriate to divide the sample into three large intervals: an initial interval, characterized by solid volatility; a second interval characterized by very low volatility, which would go up to 2019; and finally, a third interval in which there is again intense volatility, which would be the period marked by COVID-19 and the war in Ukraine. In the future, one can divide the sample into the above three intervals and select other relevant indicators for the BDI forecasting studies.
(4) In the empirical analysis, we modelled analysis of momentous events (Financial Crisis and COVID-19) that have occurred. In the future, as we stand at the threshold of an entirely new crisis, the relevance of historical events and the prophecies of global authorities will inform us to grasp the critical nodes. Subsection 5.1.1 provides strong evidence for this point.
(5) Combinatorial modeling is now considered a popular approach in forecasting, as previously mentioned. The subsequent research can create a more efficient and accurate combination model by integrating the Prophet model with other models (such as neural network) to forecast the results.

CRediT authorship contribution statement

Wenyang Wang: Conceptualization, Methodology, Writing – review & editing, Writing – original draft, Funding acquisition. **Nan He:** Data curation, Writing – original draft, Visualization, Writing – review & editing, Methodology. **Muxin Chen:** Writing – original draft, Visualization, Writing – review & editing. **Peng Jia:** Supervision, Funding acquisition.

Declaration of competing interest

The authors declare that they have no known competing financial interests or personal relationships that could have appeared to influence the work reported in this paper.

Data availability

The dataset used in the present paper is partly shared in Appendix C.

Acknowledgement

This work is supported by the Humanities and Social Science Fund of Ministry of Education of China (22YJC910011), the Postdoctoral Research foundation of China (2023M733444), the National Natural Science Foundation of China (72174035, 71774018), and the Liaoning Revitalization Talents Program, China (XLYC2008030).

The authors gratefully acknowledge the very constructive comments of the editor and the anonymous referees.

Appendix A. Comparison of the remaining variables added in Period I

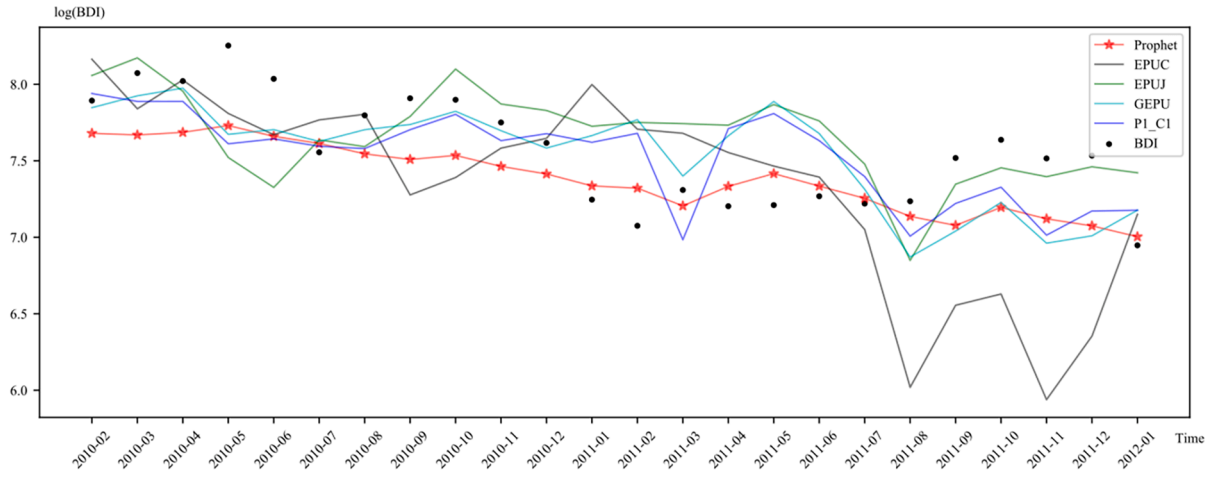

Fig. 19. Forecasting comparison of the fourth gradient variables (without considering the Financial Crisis).

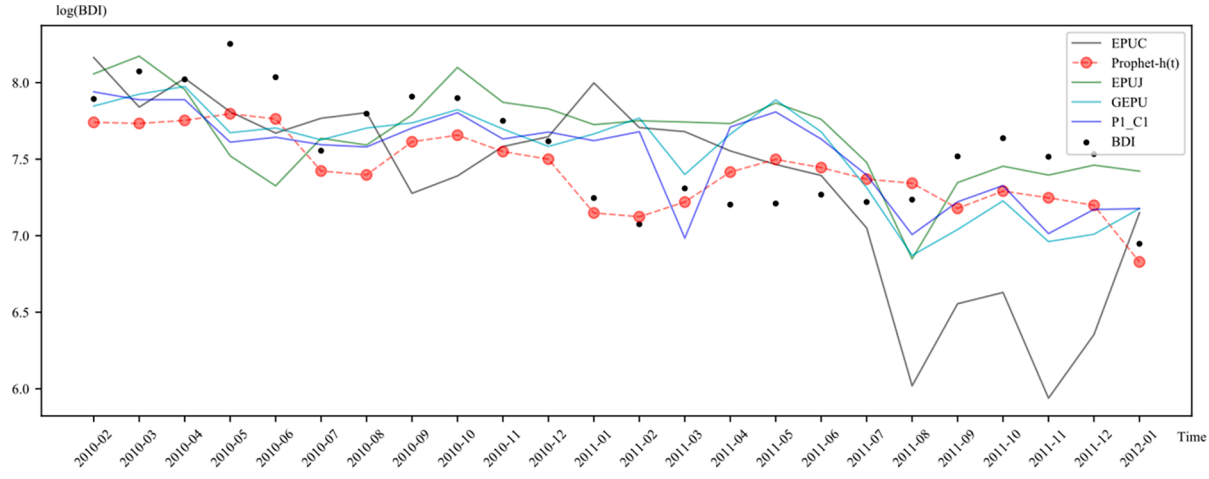

Fig. 20. Forecasting comparison of the fourth gradient variables (considering the Financial Crisis).

Appendix B. Comparison of the remaining variables added in Period II

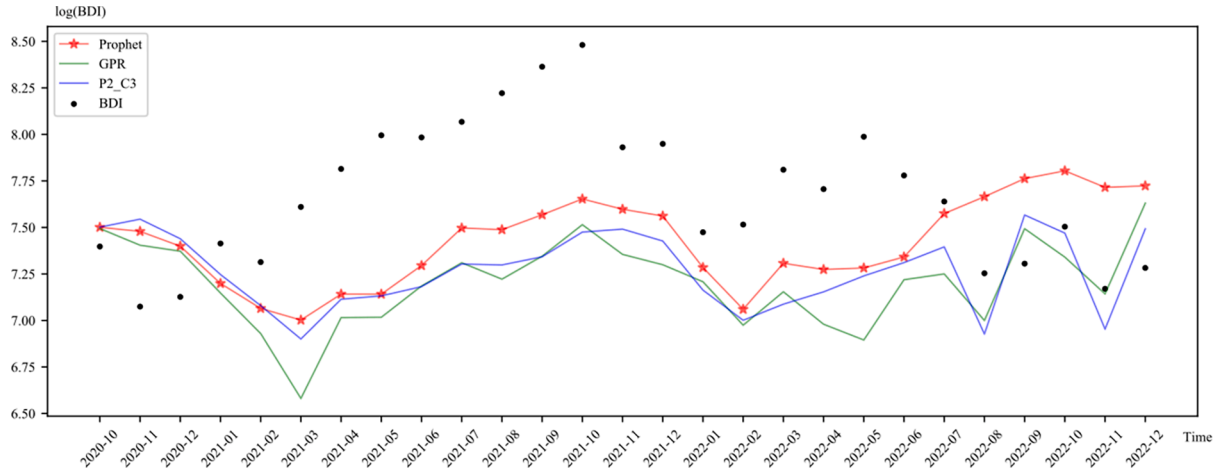

Fig. 21. Forecasting comparison of the fourth gradient variables (without considering the COVID-19).

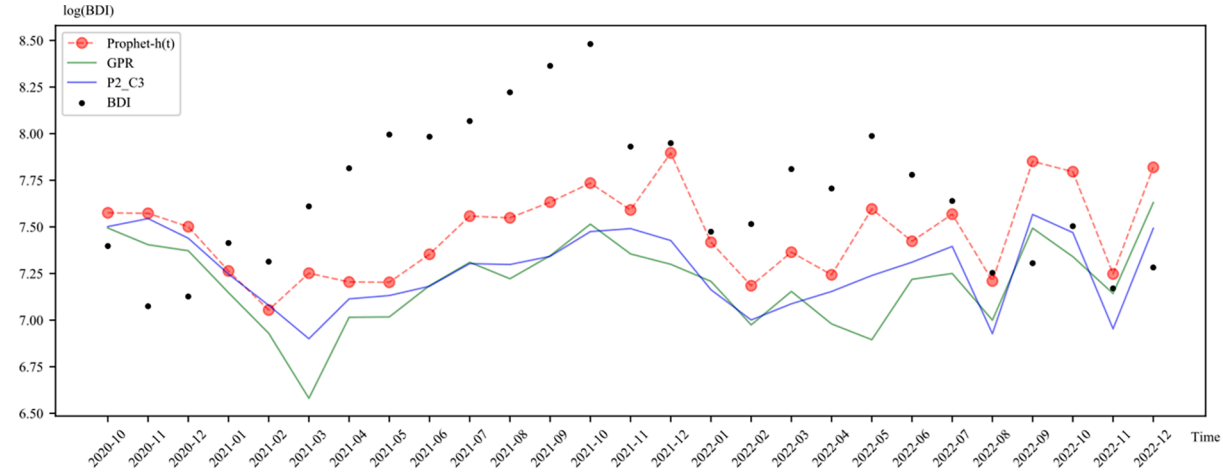

Fig. 22. Forecasting comparison of the fourth gradient variables (considering the COVID-19).

Appendix C. Data availability

Supplementary data to this article can be found online on the author's GitHub repository: https://github.com/JanisaHe.

References

Adland, R., & Cullinane, K. (2006). The non-linear dynamics of spot freight rates in tanker markets. *Transportation Research Part E: Logistics and Transportation Review, 42*(3), 211–224.

Adland, R., Cariou, P., & Wolff, F. C. (2016). The influence of charterers and owners on bulk shipping freight rates. *Transportation Research Part E: Logistics and Transportation Review, 86*, 69–82.

Alizadeh, A. H., & Talley, W. K. (2011a). Microeconomic determinants of dry bulk shipping freight rates and contract times. *Transportation, 38*, 561–579.

Alizadeh, A. H., & Talley, W. K. (2011b). Vessel and voyage determinants of tanker freight rates and contract times. *Transport Policy, 18*(5), 665–675.

Bai, X., Lam, J. S. L., & Jakher, A. (2021). Shipping sentiment and the dry bulk shipping freight market: New evidence from newspaper coverage. *Transportation Research Part E: Logistics and Transportation Review, 155*, Article 102490.

Baker, S. R., Bloom, N., & Davis, S. J. (2016). Measuring economic policy uncertainty. *The Quarterly Journal of Economics, 131*(4), 1593–1636.

Batchelor, R., Alizadeh, A., & Visvikis, I. (2007). Forecasting spot and forward prices in the international freight market. *International Journal of Forecasting, 23*(1), 101–114.

Bildirici, M., Şahin Onat, I., & Ersin, Ö.Ö. (2023). Forecasting BDI Sea Freight Shipment Cost, VIX Investor Sentiment and MSCI Global Stock Market Indicator Indices: LSTAR-GARCH and LSTAR-APGARCH Models. *Mathematics, 11*(5), 1242.

Bouri, E., Gupta, R., & Rossini, L. (2022). The role of the monthly ENSO in forecasting the Daily Baltic Dry Index. In *The role of the monthly ENSO in Forecasting the Daily Baltic Dry Index: Bouri, Elie| uGupta, Rangan| uRossini, Lua*. Pretoria, South Africa: Department of Economics, University of Pretoria.

Chaturvedi, S., Rajasekar, E., Natarajan, S., & McCullen, N. (2022). A comparative assessment of SARIMA, LSTM RNN and Fb Prophet models to forecast total and peak monthly energy demand for India. *Energy Policy, 168*, Article 113097.

Chen, F., Miao, Y., Tian, K., Ding, X., & Li, T. (2017). Multifractal cross-correlations between crude oil and tanker freight rate. *Physica A: Statistical Mechanics and Its Applications, 474*, 344–354.

Chen, Y., Liu, B., & Wang, T. (2021). Analysing and forecasting China containerized freight index with a hybrid decomposition–ensemble method based on EMD, grey wave and ARMA. *Grey Systems: Theory and Application, 11*(3), 358–371.

Cheng, S. H., Chen, S. M., & Jian, W. S. (2016). Fuzzy time series forecasting based on fuzzy logical relationships and similarity measures. *Information Sciences, 327*, 272–287.

Cullinake, K. (1992). A short adaptive forecasting modal for BIFFEX speculation: A Box-Jenkins approach. *Maritime Policy & Management, 2*, 91–114.

Dai, S., Zeng, Y., & Chen, F. (2016). The scaling behavior of bulk freight rate volatility. *The Scaling Behavior of Bulk Freight Rate Volatility*, 85–104.

Drobetz, W., Gavriilidis, K., Krokida, S. I., & Tsouknidis, D. (2021). The effects of geopolitical risk and economic policy uncertainty on dry bulk shipping freight rates. *Applied Economics, 53*(19), 2218–2229.

Duru, O. (2010). A fuzzy integrated logical forecasting model for dry bulk shipping index forecasting: An improved fuzzy time series approach. *Expert Systems with Applications, 37*(7), 5372–5380.

Duru, O., Bulut, E., & Yoshida, S. (2012). A fuzzy extended DELPHI method for adjustment of statistical time series prediction: An empirical study on dry bulk freight market case. *Expert Systems with Applications, 39*(1), 840–848.

Fahiman, F., Erfani, S. M., Rajasegarar, S., Palaniswami, M., & Leckie, C. (2017). May). Improving load forecasting based on deep learning and K-shape clustering. In *In 2017 International Goint on Neural Networks (IJCNN)* (pp. 4134–4141).

Gu, B., & Liu, J. (2022). Determinants of dry bulk shipping freight rates: Considering Chinese manufacturing industry and economic policy uncertainty. *Transport Policy, 129*, 66–77.

Guo, J., Long, S., & Luo, W. (2022). Nonlinear effects of climate policy uncertainty and financial speculation on the global prices of oil and gas. *International Review of Financial Analysis, 83*, Article 102286.

Gao, R., Zhao, Y., & Zhang, B. (2023). Baltic dry index and global economic policy uncertainty: Evidence from the linear and nonlinear Granger causality tests. *Applied Economics Letters, 30*(3), 360–366.

Gu, Y., Chen, Z., & Lien, D. (2019). Baltic Dry Index and iron ore spot market: Dynamics and interactions. *Applied Economics, 51*(35), 3855–3863.

Hao, J., Yuan, J., Wu, D., Xu, W., & Li, J. (2023). A dynamic ensemble approach for multi-step price prediction: Empirical evidence from crude oil and shipping market. *Expert Systems with Applications, 234*, Article 121117.

Hartigan, J. A., & Wong, M. A. (1979). Algorithm AS 136: A k-means clustering algorithm. *Journal of the Royal Statistical Society. Sseries C (Applied Statistics), 28*(1), 100–108.

Jing, L., Marlow, P. B., & Hui, W. (2008). An analysis of freight rate volatility in dry bulk shipping markets. *Maritime Policy & Management, 35*(3), 237–251.

Kamal, I. M., Bae, H., Sunghyun, S., & Yun, H. (2020). DERN: Deep ensemble learning model for short-and long-term prediction of baltic dry index. *Applied Sciences, 10*(4), 1504.

Katris, C., & Kavussanos, M. G. (2021). Time series forecasting methods for the Baltic dry index. *Journal of Forecasting, 40*(8), 1540–1565.

Kavussanos, M. G., & Alizadeh-M, A. H. (2001). Seasonality patterns in dry bulk shipping spot and time charter freight rates. *Transportation Research Part E: Logistics and Transportation Review, 37*(6), 443–467.

Kavussanos, M. G., & Alizadeh-M, A. H. (2002). Seasonality patterns in tanker spot freight rate markets. *Economic Modelling, 19*(5), 747–782.

Khan, K., Su, C. W., Tao, R., & Umar, M. (2021). How do geopolitical risks affect oil prices and freight rates? *Ocean & Coastal Management, 215*, Article 105955.

Klovland, J. T. (2002). *Business cycles, commodity prices and shipping freight rates: Some evidence from the pre-WWI period*. Bergen: Institute for Research in Economics and Business Administration.

Kursa, M. B., & Rudnicki, W. R. (2010). Feature selection with the Boruta package. *Journal of Statistical Software, 36*, 1–13.

Li, X., Zhang, X., Zhang, C., & Wang, S. (2024). Forecasting tourism demand with a novel robust decomposition and ensemble framework. *Expert Systems with Applications, 236*, Article 121388.

Li, Z., Piao, W., Wang, L., Wang, X., Fu, R., & Fang, Y. (2022). China coastal bulk (Coal) freight index forecasting based on an integrated model combining ARMA, GM and BP model optimized by GA. *Electronics, 11*(17), 2732.

Lin, G., Lin, A., & Gu, D. (2022). Using support vector regression and K-nearest neighbors for short-term traffic flow prediction based on maximal information coefficient. *Information Sciences, 608*, 517–531.

Liu, J., Li, Z., Sun, H., Yu, L., & Gao, W. (2022). Volatility forecasting for the shipping market indexes: An AR-SVR-GARCH approach. *Maritime Policy & Management, 49*(6), 864–881.

Luo, Z., Guo, W., Liu, Q., & Zhang, Z. (2021). A hybrid model for financial time-series forecasting based on mixed methodologies. *Expert Systems, 38*(2), e12633.

Lücke, J., & Forster, D. (2019). k-means as a variational EM approximation of Gaussian mixture models. *Pattern Recognition Letters, 125*, 349–356.

Mann, H. B., & Whitney, D. R. (1947). On a test of whether one of two random variables is stochastically larger than the other. *The Annals of Mathematical Statistics*, 50–60.

McPhail, L. L., Du, X., & Muhammad, A. (2012). Disentangling corn price volatility: The role of global demand, speculation, and energy. *Journal of Agricultural and Applied Economics, 44*(3), 401–410.

Michail, N. A., & Melas, K. D. (2020). Shipping markets in turmoil: An analysis of the Covid-19 outbreak and its implications. *Transportation Research Interdisciplinary Perspectives, 7*, Article 100178.

Mo, J., Gao, R., Liu, J., Du, L., & Yuen, K. F. (2022). Annual dilated convolutional LSTM network for time charter rate forecasting. *Applied Soft Computing, 126*, Article 109259.

Nemani, S., Cote, D., Misiuk, B., Edinger, E., Mackin-McLaughlin, J., Templeton, A., … Robert, K. (2022). A multi-scale feature selection approach for predicting benthic assemblages. *Estuarine, Coastal and Shelf Science, 277*, Article 108053.

Notteboom, T., Pallis, T., & Rodrigue, J. P. (2021). Disruptions and resilience in global container shipping and ports: The COVID-19 pandemic versus the 2008–2009 financial crisis. *Maritime Economics & Logistics, 23*, 179–210.

Papailias, F., Thomakos, D. D., & Liu, J. (2017). The Baltic Dry Index: Cyclicalities, forecasting and hedging strategies. *Empirical Economics, 52*, 255–282.

Paparrizos, J., & Gravano, L. (2015). May). k-shape: Efficient and accurate clustering of time series. In *In Proceedings of the 2015 ACM SIGMOD International Conference on Management of Data* (pp. 1855–1870).

Pepur, P., Peronja, I., & Laća, S. (2022). Global market factors that impact Baltic Dry Index. *Pomorstvo, 36*(2), 242–248.

Poblacion, J. (2015). The stochastic seasonal behavior of freight rate dynamics. *Maritime Economics & Logistics, 17*, 142–162.

Reshef, D. N., Reshef, Y. A., Finucane, H. K., Grossman, S. R., McVean, G., Turnbaugh, P. J., … Sabeti, P. C. (2011). Detecting novel associations in large data sets. *Science, 334*(6062), 1518–1524.

Rožić, T., Naletina, D., & Zając, M. (2022). Volatile freight rates in maritime container industry in times of crises. *Applied Sciences, 12*(17), 8452.

Siddiqui, A. W., & Basu, R. (2020). An empirical analysis of relationships between cyclical components of oil price and tanker freight rates. *Energy, 200*, Article 117494.

Şahin, B., Gürgen, S., Ünver, B., & Altin, I. (2018). Forecasting the Baltic Dry Index by using an artificial neural network approach. *Turkish Journal of Electrical Engineering and Computer Sciences, 26*(3), 1673–1684.

Satrio, C. B. A., Darmawan, W., Nadia, B. U., & Hanafiah, N. (2021). Time series analysis and forecasting of coronavirus disease in Indonesia using ARIMA model and PROPHET. *Procedia Computer Science, 179*, 524–532.

Schramm, H. J., & Munim, Z. H. (2021). Container freight rate forecasting with improved accuracy by integrating soft facts from practitioners. *Research in Transportation Business & Management, 41*, Article 100662.

Speiser, J. L., Miller, M. E., Tooze, J., & Ip, E. (2019). A comparison of random forest variable selection methods for classification prediction modeling. *Expert Systems with Applications, 134*, 93–101.

Saeed, N., Nguyen, S., Cullinane, K., Gekara, V., & Chhetri, P. (2023). Forecasting container freight rates using the Prophet forecasting method. *Transport Policy, 133*, 86–107.

Taylor, S. J., & Letham, B. (2018). Forecasting at scale. *The American Statistician, 72*(1), 37–45.

Unctad. (2022). *Review of Maritime Transport*. New York: United Nations Publications.

Veenstra, A. W., & Franses, P. H. (1997). A co-integration approach to forecasting freight rates in the dry bulk shipping sector. *Transportation Research Part A: Policy and Practice, 31*(6), 447–458.

Wilcoxon, F. (1992). Individual comparisons by ranking methods. In *Breakthroughs in Statistics: Methodology and Distribution* (pp. 196–202). Springer, New York: New York, NY.

Wilmsmeier, G., & Hoffmann, J. (2008). Liner shipping connectivity and port infrastructure as determinants of freight rates in the Caribbean. *Maritime Economics & Logistics, 10*, 130–151.

Wang, J., Niu, X., Zhang, L., Liu, Z., & Huang, X. (2023). A wind speed forecasting system for the construction of a smart grid with two-stage data processing based on improved ELM and deep learning strategies. *Expert Systems with Applications, 122487*.

Wu, Z., Mu, Y., Deng, S., & Li, Y. (2022). Spatial–temporal short-term load forecasting framework via K-shape time series clustering method and graph convolutional networks. *Energy Reports, 8*, 8752–8766.

Xu, H., Tao, B., Shu, Y., & Wang, Y. (2021). Long-term memory law and empirical research on dry bulks shipping market fluctuations. *Ocean & Coastal Management, 213*, Article 105838.

Xu, J. J., & Yip, T. L. (2012). Ship investment at a standstill? An analysis of shipbuilding activities and policies. *Applied Economics Letters, 19*(3), 269–275.

Yang, J., Ning, C., Deb, C., Zhang, F., Cheong, D., Lee, S. E., … Tham, K. W. (2017). K-Shape clustering algorithm for building energy usage patterns analysis and forecasting model accuracy improvement. *Energy and Buildings, 146*, 27–37.

Yang, Z., & Mehmed, E. E. (2019). Artificial neural networks in freight rate forecasting. *Maritime Economics & Logistics, 21*, 390–414.

Yenidoğan, I., Çayir, A., Kozan, O., Dağ, T., & Arslan, Ç. (2018, September). Bitcoin forecasting using ARIMA and PROPHET. In *2018 3rd International Conference on Computer Science and Engineering (UBMK)* (pp. 621-624).

Yin, J., & Shi, J. (2018). Seasonality patterns in the container shipping freight rate market. *Maritime Policy & Management, 45*(2), 159–173.

Yusof, U. K., Khalid, M. N. A., Hussain, A., & Shamsudin, H. (2020, December). Financial Time Series Forecasting Using Prophet. In *International Conference of Reliable Information and Communication Technology* (pp. 485-495). Cham: Springer International Publishing.

Zeng, Q., & Qu, C. (2014). An approach for Baltic Dry Index analysis based on empirical mode decomposition. *Maritime Policy & Management, 41*(3), 224–240.

Zeng, Q., Qu, C., Ng, A. K., & Zhao, X. (2016). A new approach for Baltic Dry Index forecasting based on empirical mode decomposition and neural networks. *Maritime Economics & Logistics, 18*, 192–210.

Zhang, X., Xue, T., & Stanley, H. E. (2018). Comparison of econometric models and artificial neural networks algorithms for the prediction of baltic dry index. *IEEE Access, 7*, 1647–1657.

Zhang, X., Cheng, S., Zhang, Y., Wang, J., & Wang, S. (2023). An attention-PCA based forecast combination approach to crude oil price. *Expert Systems with Applications, 122463*.

Zhao, H. M., He, H. D., Lu, K. F., Han, X. L., Ding, Y., & Peng, Z. R. (2022). Measuring the impact of an exogenous factor: An exponential smoothing model of the response of shipping to COVID- 19. *Transport Policy, 118*, 91–100.